FLORIDA STATE UNIVERSITY

COLLEGE OF ARTS AND SCIENCES

FLASH DROUGHTS IN THE WAKE OF LANDFALLING ATLANTIC TROPICAL CYCLONES

By

TYLER JOHN MICHAEL SHERROD

A Thesis submitted to the
Department of Earth, Ocean, and Atmospheric Science
in partial fulfillment of the
requirements for the degree of
Master of Science

2022

Tyler Sherrod defended this thesis on March 3, 2022.
The members of the supervisory committee were:

Vasubandhu Misra
Professor Directing Thesis

Robert Hart
Committee Member

Henry Fuelberg
Committee Member

The Graduate School has verified and approved the above-named committee members, and certifies that the thesis has been approved in accordance with university requirements.

I dedicate this thesis to my father: Michael Sherrod; mother: Bobbie Sherrod; and siblings: Trent Sherrod, Justin Sherrod, and Hannah Sherrod. I also dedicate this thesis to my girlfriend, Sydney Giesen, and to my friends at Florida State University and in Melbourne, Florida. Without their support this thesis would not be possible.

ACKNOWLEDGMENTS

I acknowledge the support from the NASA grant 80NSSC19K1199.

TABLE OF CONTENTS

LIST OF FIGURES

ABSTRACT

A new methodology has been introduced to detect flash droughts. This method is based off a new variable created called the drought index. This index is calculated using the cumulative daily anomalies of soil moisture, precipitation, and surface temperature. The viability of this methodology is tested using confirmed flash drought case studies from previous studies. The advantage of the drought index is that it allows for the identification of the flash drought period in a more objective manner than earlier studies.

While relatively uncommon, it is possible for flash droughts to develop in the environment created post-landfall of an Atlantic Tropical Cyclone (TC). The new flash drought detection method created was then used to detect flash droughts in the wake of landfalling Atlantic TCs. Of the thirty landfalling Atlantic TCs examined between 2000 and 2018, only four cases resulted in the development of a flash drought. Despite TCs causing an increase in soil moisture, the decrease in precipitation and increase in surface temperature post-landfall in these four cases resulted in the development of a flash drought. When these flash droughts did occur, it was in conjunction with an already existing large-scale drought in the vicinity of the landfall. This suggests that the flash droughts extended the reach of the large-scale droughts to the landfall region of the TC.

1. INTRODUCTION

1.1 – Flash Drought Definition and Development

Droughts can have devastating impacts for the regions where they develop. Extreme drought events in the United States can cause disruptions and damage to society, natural ecosystems, surface and groundwater supplies, and agricultural production (Otkin et al. 2018). A common perception of drought is that it is a slowly evolving phenomenon, whose impacts are non-structural and spread over a comparatively large geographical area. Furthermore, unlike other natural hazards, the inception, maturity, and demise of droughts are not easy to assess. Whenever drought impacts are assessed, they already are well underway or have passed. However, recent studies have introduced the concept of a rapidly developing drought, called the flash drought (e.g., Hunt et al. 2014, Otkin et al. 2013, 2018). They are characterized by rapid intensification of a drought that initially begins as a meteorological drought but then transitions to an agricultural drought (Christian et al. 2019). A meteorological drought refers to a precipitation deficit over a time period while accounting for local climatological differences (Otkin et al. 2018). An agricultural drought refers to plant and crop water requirements not being met during the growing season, resulting in reduced plant and crop yield (Otkin et al. 2018).

The term “flash drought” has become more popular in the scientific community in recent years, but there is a lack of consistency regarding the exact definition of a flash drought. Two distinct approaches have been used to describe flash droughts in the scientific community: one is based on the rate of intensification of the flash drought and the other is based on the intensity of the flash drought (Otkin et al. 2018). However, Otkin et al. (2018) suggest that the definition of a flash drought should focus on the rate of intensification of the drought instead of the duration of the drought. Since an event that lasts only a few days and has minimal impacts would not be

considered a drought event, it should not be classified as a flash drought event either (Otkin et al. 2018). Longevity and impact are characteristics of any type of drought. The quality that differentiates a flash drought from an ordinary drought is the rapid rate at which the drought develops and intensifies. This definition proposed by Otkin et al. (2018) that focuses on the rapid rate of intensification of the drought will be the flash drought definition used for the purposes of this thesis.

Deficit in precipitation is a basic requirement for all droughts, but its presence alone is not enough to lead to a flash drought (Otkin et al. 2018). Above-normal evaporation must also be present for drought conditions to rapidly emerge (Otkin et al. 2018). Above-normal evaporation may occur due to high temperatures, low humidity, strong winds, and clear skies (Otkin et al. 2018). However, these conditions do not all have to be present at the same time for above-normal evaporation to occur. The combination of a deficit in precipitation and above-normal evaporation leads to a soil moisture deficit due to the evaporative demand and a lack of precipitation to replenish the removed soil moisture (Otkin et al. 2018). If these conditions are present for an extended period, a drought will quickly develop.

The evolution of a flash drought is depicted in Fig. 1.1, which is borrowed from Otkin et al. (2018). Below normal precipitation and above average atmospheric demand lead to enhanced evapotranspiration and result in a depletion in soil moisture (Fig. 1.1). Low root zone soil moisture causes evapotranspiration to decrease (Fig. 1.1). From there, vegetation and ecological health will deteriorate, and an agricultural drought will begin (Fig. 1.1).

1.2 – Impact of Flash Drought

Flash droughts have the capability of becoming much more devastating than a typical drought event. The rapid manifestation of droughts can severely impact ecosystems, agricultural productivity, manifest as heat waves, cause increased risk of wildfire development, deplete water resources, and reduce air quality, causing a threat to public health (Anderson et al. 2013; Otkin et al. 2013; Mo and Lettenmaier 2015; McEvoy et al. 2016; Wang et al. 2016; Yuan et al. 2018; Christian et al. 2019; Nguyen et al. 2019; Christian et al. 2021). The 2017 flash drought across the U.S. Northern Plains and Canadian Prairies can help illustrate some of these impacts. Through late April and early May, conditions were warm and moist in Montana which would be beneficial for the growing season (Jencso et al. 2019). However, above-normal temperatures and wind speeds from the onset of the flash drought resulted in a decrease in soil moisture, and crop conditions deteriorating by late May (Jencso et al. 2019). The area of Montana's 2017 fire season was the largest in the past 100 years (Jensco et al. 2019). Approximately 1.4 million acres and 2420 individual fires burned across Montana during the 2017 fire season, resulting in the loss of food for wildlife and livestock, crop loss, injury to human health, and lost tourism revenue (Jensco et al. 2019). Smoke from the wildfires also resulted in a deterioration of air quality in Montana and negatively impacted human health. During the month of August 2017, there was not a single day where all monitoring stations in Montana reported good air quality (Jensco et al. 2019). Water shortages were not a significant issue during the 2017 flash drought event, but water shortages were experienced in the Canadian Prairies and by tribal nations in South Dakota (Jensco et al. 2019).

Analyzing maps from the United States Drought Monitor (USDM) in conjunction with this flash drought event in the U.S. Northern Plains and Canadian Prairies help to illustrate how

quickly the flash drought developed. Fig. 1.2, borrowed from Hoell et al. (2020), depicts the USDM maps throughout the development of this flash drought event. The drought category level increased from sporadic abnormal dryness at the end of April to extreme and exceptional drought throughout Montana, North Dakota, and South Dakota by the end of July (Fig. 1.2). The USDM is not the only tool for detecting flash drought, and it does not always indicate a flash drought situation due to there being some subjectivity in the way that the organization determines when a drought event is occurring. However, it is a good tool to use initially to develop an idea of how quickly a drought is developing. Fig. 1.3, also borrowed from Hoell et al. (2020), presents the factors that assisted this flash drought in developing quickly. From May to July, there was a large decrease in soil moisture, a negative soil moisture anomaly, and a positive maximum temperature anomaly in the U.S. Northern Great Plains (Fig. 1.3). In any drought situation, the persistent presence of these three variables will allow the drought to rapidly develop. The three variables also play a significant role in the development of the drought index used in this thesis.

Mo and Lettenmaier (2015) hypothesize that there are two types of flash droughts: heat wave flash droughts and precipitation deficit flash droughts. Heat wave flash droughts typically occur when high temperatures cause an increase in evapotranspiration and a decrease in soil moisture. The lack of precipitation is important but not the major reason why the flash drought occurs (Mo and Lettenmaier 2015). Precipitation deficit flash droughts result from a lack of precipitation that then causes a decrease in evapotranspiration and an increase in temperatures (Mo and Lettenmaier 2015). Heat wave flash droughts are particularly devastating for the agricultural sector, where crop and livestock losses can have huge economic ramifications. They are most likely to occur in the Midwest during the growing season (Mo and Lettenmaier 2015).

1.3 – Flash Drought Hot Spots and Detection Methods

In a recent study using reanalysis data, Christian et al. (2021) identified large portions of Brazil, Sahel, the Great Rift Valley, and India as hot spots for flash droughts. These regions exhibited a frequency of occurrence of flash drought between 30 to 40% over a 36-year period. They also noted secondary hotspots of flash droughts over the central and mid-western United States and central Mexico in North America. They attributed these hot spots of flash drought to strong land-atmosphere coupling, wherein the drying land surface rapidly translates to drying of the overlying atmospheric column. The opposite can be true as well, where a drying atmospheric column can cause drying of the land below. The positive feedback of decreased soil moisture, less evapotranspiration into the atmosphere lowering the precipitation potential, and increased surface temperature results in a greater likelihood of flash drought occurrence (Christian et al. 2021). Land-atmosphere coupling could be an important precursor to flash droughts, especially in regions on the edge of climate transition zones that are more susceptible and sensitive to coupling dynamics (Christian et al. 2021). Mei and Wang (2012) found the Great Plains to be a hot spot for strong land-atmosphere coupling, with the Midwest and Southeast also exhibiting strong land-atmosphere coupling. This is important to note because many of the flash droughts that will be analyzed in this thesis occur in these regions.

Several studies suggest that the United States is one of the most affected countries by both floods and droughts (Villarini et al. 2011; Retchless et al. 2014). Zhou et al. (2018) estimate that in the decades between 1996 and 2016, the economic costs of 6520 floods per year was 3.986 billion US dollars per year while the average cost of 2427 droughts per year was 1.684 billion US dollars per year. The NOAA National Centers for Environmental Information actually calculates that annual losses associated with droughts nears about $9 billion per year (NOAA

n.d.). Over the past three decades, droughts have ranked as the second costliest billion-dollar weather disasters (NOAA n.d.).

The USDM is the organization that evaluates drought and flash drought conditions using a variety of sources such as monitoring indices, soil moisture conditions, hydrological data, and information from qualified observers (Misra 2020). Other researchers have devised their own methods to detect flash droughts. Hunt et al. (2014) utilized two different drought indices, the Standard Precipitation Index (SPI) and the Standardized Precipitation Evapotranspiration Index (SPEI), to show how short-term drought indices could successfully be used to detect flash droughts by looking at precipitation and evapotranspiration trends. The SPI calculates the number of standard deviations that observed precipitation anomalies stray from the long-term precipitation mean (Keyantash et al. 2018). Since the SPI has the limitation of not accounting for evapotranspiration (and temperature as a direct result), the SPEI was developed to also consider evapotranspiration. Both the SPI and SPEI have the limitation of needing to rely on 30-50 years of data to model what drought conditions will look like in the future (Keyantash et al. 2018). Otkin et al. (2013) make use of the evaporative stress index (ESI), which estimates evapotranspiration using remotely sensed IR images. The ESI is calculated using a thermal-infrared-based surface energy balance model called Atmospheric Land Exchange Inverse (Otkin et al. 2013). This model can estimate evapotranspiration by remotely sensing the morning increase of the land surface temperature in the contiguous US (Otkin et al. 2013). The final ESI calculation is done by determining the ratio of evapotranspiration to potential evapotranspiration (Otkin et al. 2013). Results determined that ESI can be used to detect the rapid onset of a flash drought before the USDM can (Otkin et al. 2013). Christian et al. (2019) developed their own methodology for flash drought detection based on the flash drought definition proposed by Otkin

et al. (2018). This study uses the Evaporative Stress Ratio (ESR) to identify flash drought cases. The ESR is like the SPEI in that it is calculated using the ratio of evapotranspiration to potential evapotranspiration (Christian et al. 2019). Unfortunately, the ESR also has the same issue as earlier indices, being reliant upon modeled data. A major disadvantage shared by all the flash drought detection methods is that they cannot identify a flash drought using directly observed and analyzed variables. This disadvantage prevents flash drought events from being monitored or forecast in real-time and serves as motivation for developing our own flash drought index.

1.4 – Link Between Tropical Cyclones and Flash Drought

Landfalling tropical cyclones (TCs) cause some of the costliest damage to the nation, largely from flooding and wind damage. However, far less attention has been paid to the post-landfall period when the likelihood of a sustained dry and warm period can cause human misery, fatalities, and lead to collateral losses. In many of these cases, the heat stress from high wet bulb temperatures in the days after landfall become life threatening, as was evident from the tragic deaths from heat stress during the post-Hurricane Irma (2017) period in Hollywood, Florida (Berman et al. 2017).

Studies by Scoccimarro et al. (2020) and Sobel and Camargo (2005) suggest that tropical cyclones can induce drought-like conditions to nearby regions while passing through. For example, Sobel and Camargo (2005) found that the large-scale environment in the primary region of TC activity, lagging the accumulated cyclone energy by about two weeks, becomes far less conducive for cyclogenesis due to the reduction of sea-surface temperature (SST) and precipitable water, and an increase in outgoing longwave radiation. In other words, tropical cyclones induce a SST reduction in the primary region of tropical cyclone activity in the Western North Pacific (WNP) (Sobel and Camargo 2005). These tropical cyclones also induce cooling,

drying, and a reduction of outgoing longwave radiation in a zone partially overlapping the primary region of tropical cyclone activity. However, these conditions are primarily induced to the south and west of the region of primary tropical cyclone activity (Sobel and Camargo 2005). Some of these conditions, like the reduction of precipitable water and an increase of outgoing longwave radiation over land can also lead to the rapid intensification of drought. Scoccimarro et al. (2020) found that there is a significant negative correlation between the WNP Accumulated Cyclone Energy (ACE) and precipitation over the Maritime Continent. In fact, Scoccimarro et al. (2020) showed that the typhoon induced drying of the Maritime Continent results in the onset of their dry season. They found that TCs induce a net moisture flux divergence over the Maritime Continent, leading to the onset of their dry season. Scoccimarro et al. (2020) suggest that a possible explanation is that tropical cyclones can cause eastward wind anomalies at lower latitudes that transport vertically integrated water content away from the Maritime Continent. During high ACE years (i.e., an active tropical cyclone season), there is less water available for local precipitation over the Maritime Continent (Scoccimarro et al. 2020).

A study by Schenkel and Hart (2015) also came to a similar conclusion as Sobel and Camargo (2005) and Scoccimarro et al. (2020) about WNP TCs and their impact on the large-scale environment around them. They found that large TCs can cause cooling and drying to their synoptic-scale environment for approximately 40 days. This cooling and drying is caused by a combination of the TC, TC-induced Rossby waves, and the Madden-Julian Oscillation (MJO) (Schenkel and Hart 2015). TC-induced Rossby waves discharged from the south and east of TCs were found to likely cause westward propagation of anomalous cooling and drying of the environment (Schenkel and Hart 2015). It was found that favorable environments for TC-induced Rossby wave dispersion resulted in stronger cooling and drying of the environment in

the wake of a TC (Schenkel and Hart 2015). These TC-induced Rossby waves are triggered in large TCs but absent in smaller TCs (Schenkel and Hart 2015). Additionally, the region of negative SST anomalies is greater for large TCs and is lesser for small TCs (Schenkel and Hart 2015). The cooling and drying of the synoptic-scale environment results in unfavorable conditions for future TCs. This study along with Scoccimarro (2020) and Sobel and Camarago (2005) focus on the WNP, but the results from both studies reveal that TCs can have an impact the dynamics of other environments that they pass through.

1.5 – Thesis Objectives

The main objective of this thesis is to determine the incidence of flash droughts over the United States (US) from landfalling Atlantic tropical cyclones. This objective is motivated by the studies conducted over the WNP, which exhibit similar impacts from tropical cyclones (Sobel and Camargo 2005; Scoccimarro et al. 2020). To fulfill the objective, we introduce a new methodology to detect flash drought, which is simple and easier to implement than some of the existing definitions. This methodology is verified with historical, documented flash droughts by the USDM. Following this verification, we then examine all cases of landfalling Atlantic tropical cyclones in the US between the years of 2000 and 2018 for flash droughts.

For the first time, we are attempting to diagnose incidence of flash droughts from landfalling Atlantic TCs. Unfortunately, the legacy of officially diagnosing flash droughts has resided with the USDM, wherein they look at rapid deterioration of the drought categories to posteriorly claim the occurrence of flash drought. Their flash drought categories are based off coarse analysis and is subjectively modified based on consultation with local state climatologists, drought monitors, and water resource managers, However, to diagnose incidence of flash droughts in the wake of landfalling Atlantic TCs, we must rely on relatively high-resolution data

because the size of TCs is usually small relative to the droughts of the Midwest and Western US. Furthermore, unlike the USDM flash drought definitions that are based on weekly maps, we must examine the flash drought evolution on a daily interval. Finally, we also to want to develop an index that could be easily adapted to forecast data. Therefore, there is an urgent need to propose a flash drought index that is objective. This flash drought index should be based on easily observed and analyzed variables. It should also be capable of being monitored or forecasted at a daily interval. In this regard, we propose a new drought index that meets these needs.

In the following chapter, the data used in this study and the methodology to detect flash droughts will be discussed. The results are presented in Chapters 4 and 5, wherein we show the efficacy of the methodology followed by the detection of flash drought cases after TC landfall. The concluding remarks are provided in Chapter 6.

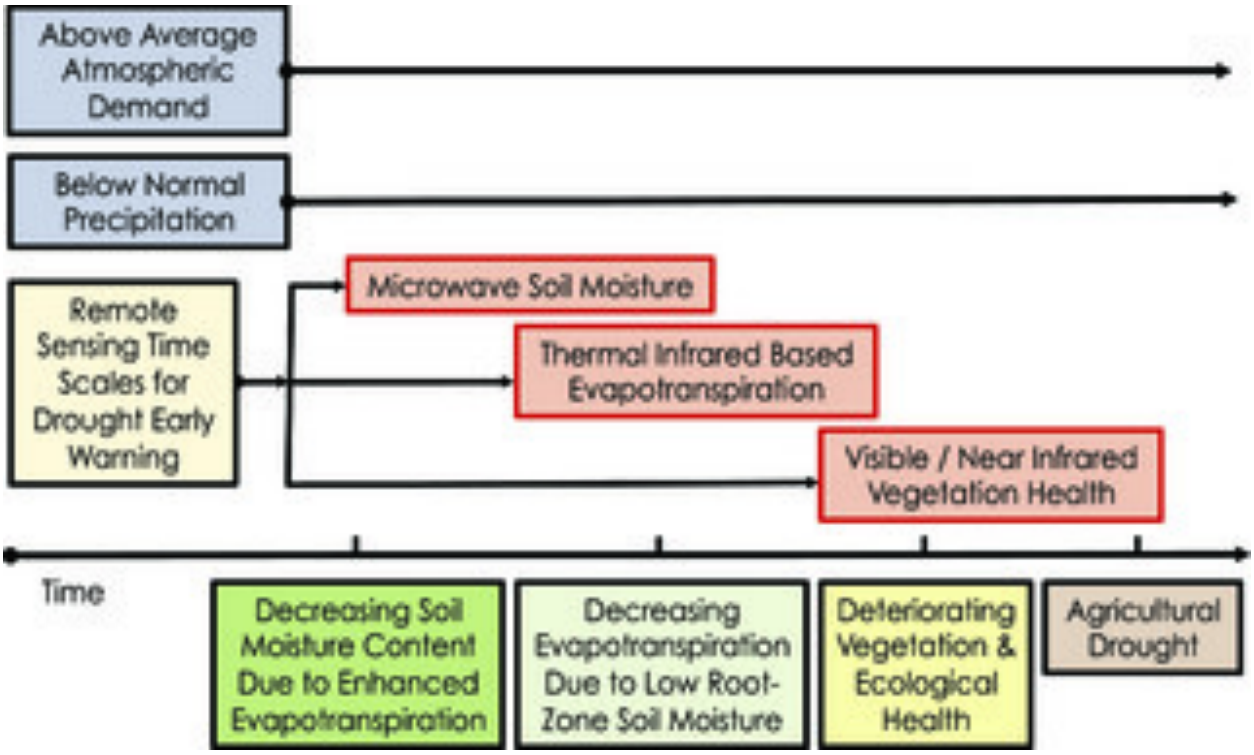

Figure 1.1: Typical evolution of a flash drought (borrowed from Otkin et al. 2018)

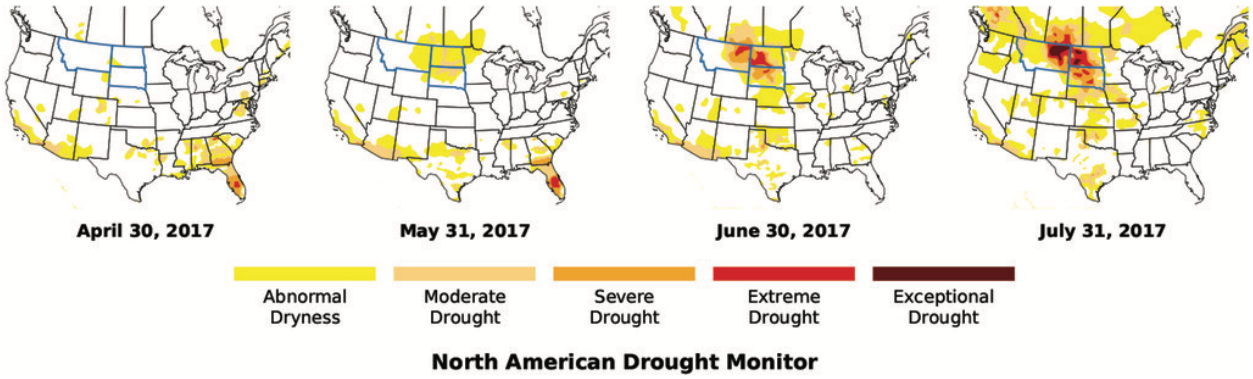

Figure 1.2: USDM maps depicting the evolution of the U.S. Northern Great Plains and Canadian Prairies flash drought from the summer of 2017 (borrowed from Hoell et al. 2020). The U.S. Northern Great Plains states of Montana, North Dakota, and South Dakota are outlined in blue.

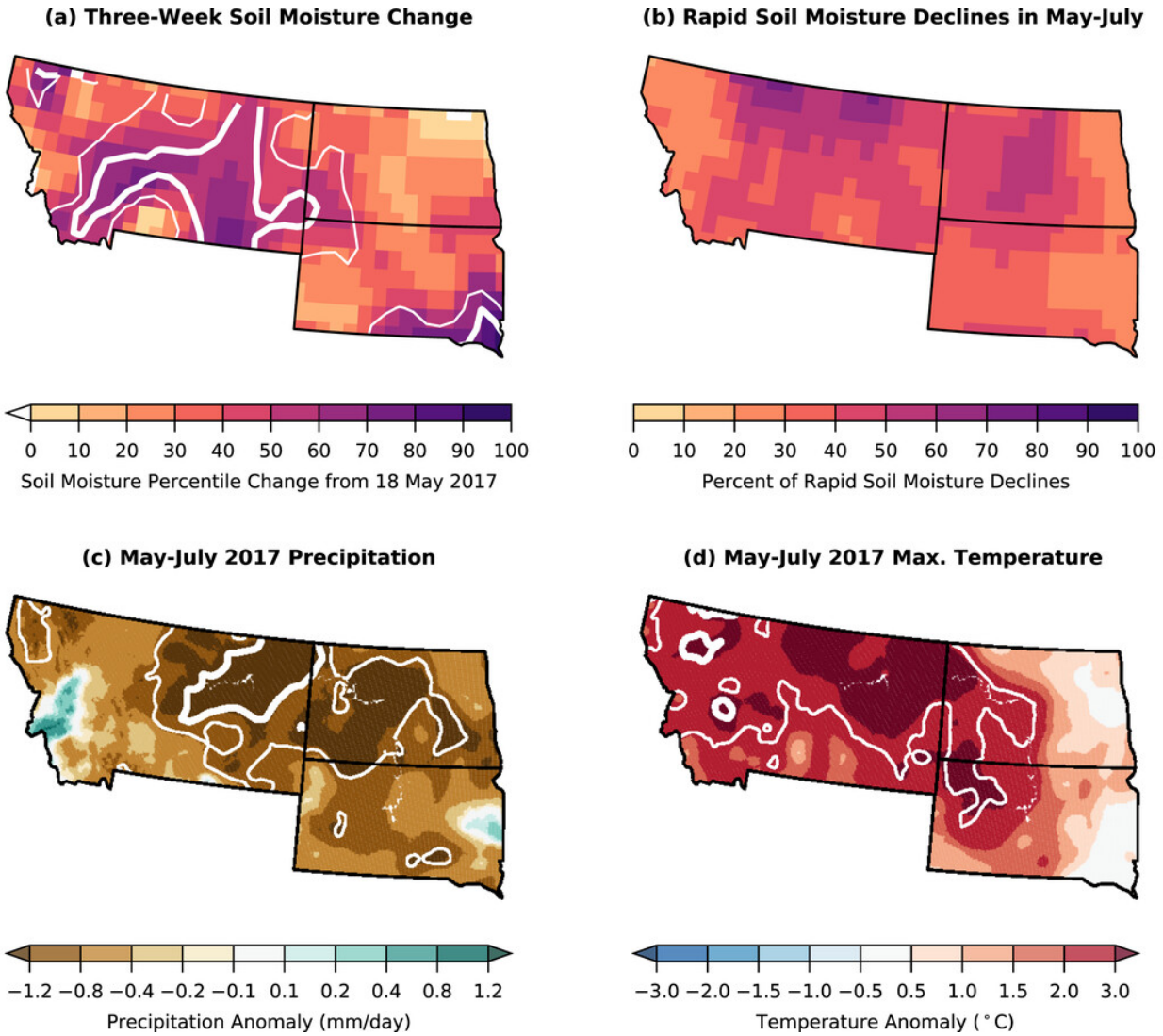

Figure 1.3: (a) The 3-week soil moisture percentile decline from 18 May 2017 (shaded) and percentile rank of the decline (contours). (b) Percentage of top 3-week soil moisture percentile declines occurring in May–July for 1916–2017. (c) May–July 2017 precipitation anomaly (shaded; mm day^{-1}) and percentile rank (contours). (d) May–July 2017 maximum temperature anomaly (°C) and percentile rank (contours). The thick and thin contours in (a), (c), and (d) indicate the top percentile and quintile, respectively. Soil moisture is based on the UCLA Surface Water Monitor. Precipitation and temperature are based on nClimGrid/CLIMGRID (Vose et al. 2014). Precipitation and temperature ranks are adapted from Hoell et al. (2019a). Figure borrowed from Hoell et al. (2020).

2. **DATA**

The data used for the detection of soil moisture in this thesis is NASA's Soil MERGE (SMERGE; doi:10.5067/PAVQY1KHTMUT) root-zone (0-40cm) soil moisture dataset. The SMERGE product is developed by merging North American Land Data Assimilation version 2 (NLDAS-2) with satellite-based moisture retrievals to produce 0.125° gridded, daily Root Zone Soil Moisture (RZSM) for the conterminous United States (Rui and Dong 2021; Rui and Mocko 2021). RZSM is the volumetric soil moisture with units of m^3m^{-3}. This dataset is in a netCDF format and spans multiple decades (January 1979 to May 2019; NASA 2021). The spatial extent of the soil moisture data is 25°N to 53°N and 67°W to 125°W. In order to merge the satellite-based soil moisture retrievals with NLDAS-2 data, the soil moisture retrievals had to be linearly interpolated from 0.25-degrees to 0.125-degrees (NASA 2021).

The data used for the detection of precipitation is the NASA Integrated Multi-Satellite Retrievals for Global Precipitation Mission (IMERG) Final Run gridded, daily, global, precipitation (Huffman et al. 2020) dataset available from 2000 to the present at 0.1° grid resolution. NASA and the Japanese Aerospace Exploration Agency (JAXA) developed the IMERG dataset together from their Global Precipitation Measurement (GPM) mission (NASA 2021). The algorithm used to create this precipitation dataset is intended to calibrate, merge, and interpolate satellite microwave precipitation estimates with other precipitation estimators (NASA 2021). These other estimators include microwave-calibrated IR satellite estimates and precipitation gauge analyses over the whole globe (NASA 2021). There are also IMERG Early Run and IMERG Late Run datasets, but the IMERG Final Run data is used because it has better fidelity as opposed to the 4-hour and 12-hour latency of the early and late runs (NASA 2021; Tang et al. 2016; Liu et al. 2016; Xu et al. 2019). The IMERGE Final Run also uses datasets

such as the MERRA2 (Gelaro et al. 2017), ERA-5 (Hersbach et al. 2019), and ERA-Interim (Dee et al. 2011) for reanalysis (Huffman et al. 2019).

The data used for the detection of surface temperature is NOAA's Climate Prediction Center gridded, daily, global, land surface temperature (NOAA 2020) dataset and is available from 1979 to the present at 0.5° grid resolution. This surface temperature is in netCDF format and spans the entire globe (NOAA 2020). The temperature data included within has a daily-temperature maxima, temperature minima, and a mean temperature (Shi 2021).

3. METHODOLOGY

Flash drought, as mentioned earlier, refers to the rapid intensification of drought, and this is the definition followed in this thesis as well. Since flash drought has a significant impact on agriculture (Hoell et al. 2020), the focus to diagnose flash drought is usually based on changes in drought indices that are computed over short time periods, and which are sensitive to soil moisture, evapotranspiration, evaporative demand, and vegetation health (Otkin et al. 2013). Some studies have shown that variables that account for the balance between supply and demand of surface moisture are better predictors of flash drought than surface temperature and precipitation by themselves (Ford and Labosier 2017; Otkin 2018). However, all these studies require the root zone soil moisture to rapidly decrease in association with flash drought (Seneviratne et al. 2010; Yuan et al. 2018).

In this study, we use the daily SMERGE root zone soil moisture along with surface temperature and precipitation to diagnose flash drought in the continental US. These variables are areal averaged over a radius of 500 km around the identified regions of the flash drought from earlier studies. Flash droughts identified from previous studies were used to develop an index in order to make the index as accurate as possible. The choice of this radius is pertinent to the case of landfalling TCs and is explained further later in the methodology. However, this choice of the radius does not influence the diagnosis of the spatial extent of the flash drought, which is explained later. We compute the daily cumulative anomaly (D_i) of soil moisture, precipitation, and temperature, separately, as:

$$D_k = \sum_{k=n}^{m} \bar{d}'_k \quad (1)$$

Where, overbar denotes area average and

$$D_k \in \begin{cases} S_k \\ P_k \\ T_k \end{cases} and\ \bar{d}'_k \in \begin{cases} \bar{s}'_k \\ \bar{p}'_k \\ \bar{t}'_k \end{cases}$$

(2)

Where, S_k, P_k, T_k are daily cumulative anomalies of soil moisture, precipitation, and temperature, $\bar{d}'$ is the daily area averaged soil moisture ($\bar{s}'$), precipitation ($\bar{p}'$), temperature ($\bar{t}'$) anomalies, k is the time index in days starting from the n^{th} day to the m^{th} day. The daily anomaly, d_k' is given by:

$$d'_k = \bar{d}_k - \bar{\bar{d}}_k$$

(3)

Where, $\bar{d}_k$ are the daily area averaged soil moisture or temperature or precipitation and $\bar{\bar{d}}_k$ represents the corresponding climatology for day *k*, respectively. The daily cumulative anomaly (D_i) curves are then normalized by their standard deviation to make them unitless:

$$\widehat{D}_k = \frac{D_k}{\sigma_D}$$

(4)

Where,

$$\widehat{D} \in \begin{cases} \hat{S}_k \\ \hat{P}_k \\ \hat{T}_k \end{cases}$$

(5)

Then a combined, normalized cumulative anomaly curve, which will be called the drought index cumulative anomaly curve ($\hat{C}_{\mathrm{k}}$) is computed as:

$$\hat{C}_k = \hat{S}_k + \hat{P}_k + (-\hat{T}_k)$$

(6)

The idea of this drought index cumulative anomaly curve is to isolate the conditions of the flash drought characterized by rapid decrease in soil moisture and precipitation and an increase in surface temperature. It will be shown in the next chapter that the flash drought period can be easily recognized from the time series of $\hat{C}_{\mathrm{k}}$ which will show a rapid decline, with negative values over the flash drought period. To gauge the spatial extent of the flash drought, we first compute $\hat{C}_{\mathrm{jk}}$ at every grid point, j, and then diagnose its temporal correlation with $\hat{C}_{\mathrm{k}}$. Then, the regions with statistically significant correlations are identified to define the spatial

extent of the flash drought. These regions of high correlation will suggest a similar temporal evolution of the drought index as in $\hat{C}_{\mathrm{k}}$.

In the first half of the next section, we will ascertain the efficacy of this methodology with known cases of flash drought, as diagnosed by the National Drought Mitigation Center using the USDM maps (Otkin et al. 2018). After testing the potency of the methodology, reliance on previous defined flash droughts is no longer needed. Subsequently, we apply this methodology to examine the incidence of flash drought in the wake of all landfalling, named Atlantic TCs from 2000-2018. In the case of landfalling TCs, the use of the effective radius of 500 km to area average soil moisture, temperature, and precipitation anomaly around the coordinates of the landfall point before the daily cumulative anomaly is computed to detect flash drought period is obvious. This radius is an optimal radius for encompassing the TC-induced precipitation shield (Jiang and Zipser 2010; Lee et al. 2010; Khouakhi et al. 2017, Zhou et al. 2018). Khouakhi et al. (2017) claims that rainfall induced by a TC should be within 500 km of the center of the TC because it is consistent with other studies (including Jiang and Zipser 2010; Lee et al. 2010; Chavas and Emanual 2010; Dare et al. 2012; Prat and Nelson 2013; Villarini et al. 2014). They also claim that the 500 km radius is a typical radius for the primary TC wind circulation and the extent of the curved TC cloud shield (Prat and Nelson 2013; Khouakhi et al. 2017). When considering the top 10% of rainiest TCs in each basin, the composite mean rainfall is heaviest in the 500 km radius around the TC (Villarini et al. 2014b; Khouakhi et al. 2017). Rainfall from the center of the TC and from rainbands are also accounted for by this 500 km radius (Dare et al. 2012, Khouakhi et al. 2017). Furthermore, the averaging of the variable over a large enough area is important to otherwise avoid detection of spurious small scale drying, which may be unrelated to the developing drought over a larger area.

The drought index has a few advantages over other existing indices to detect flash drought that were discussed in the introduction (USDM, SPI, SPEI, ESI, and ESR). The drought index can objectively define the onset and demise of a flash drought down to the exact date by analyzing the slope of the drought index during a period where a flash drought is expected to be occurring. Our index is based on observed variables as opposed to other models that rely on modeled data and the USDM that relies on subjective intervention. Creating an index based off observed variables removes the need to use sophisticated land surface models used by other methodologies to calculate evapotranspiration. Finally, the drought index is a great visualization tool that can be used to describe droughts on a spatial scale.

4. RESULTS: EFFICACY OF THE PROPOSED DROUGHT INDEX

4.1 – East Missouri Flash Drought Verification

The methodology is illustrated by examining an iconic flash drought event over the Midwestern United States, in the summer of 2012 (Otkin et al. 2018). Fig. 4.1a shows the 8-week change in the drought category of the USDM ending on 24 July 2012. The flash drought is diagnosed by a three to five category increase in drought severity over the 8-week period, as per the USDM maps (Otkin et al. 2018; Fig. 1a). The flash drought in Fig. 4.1a extends from Montana in the Northwest corner to Arkansas in the southeast and from Oklahoma in the southwest corner to Michigan in the northeast. The corresponding cumulative soil moisture anomaly, areal averaged around a radius of 500 km centered over East Missouri is shown in Fig. 4.2a. The choice of East Missouri as the center of the 500 km radius circle is chosen posteriorly from the analysis of this event in Otkin et al. (2018), which indicates East Missouri to be the center of a flash drought event (e.g., Otkin et al. 2018). Furthermore, the start of the cumulative anomaly curve from 15 April 2012, in Fig. 4.2a is also based on the earlier analysis of this flash drought event in Otkin et al. (2018) that documented the precipitous increase in drought severity over the 8-week period ending on 24 July 2012. The curve is advanced further by 6 weeks earlier to the start of the 8-week period ending on 24 July 2012, to be able to objectively diagnose the start of the flash drought event. It may be noted that the potential period of flash drought is far more apparent in the daily cumulative anomaly curve of the soil moisture when there is a steep decline from early May to September (Fig. 4.2a). In contrast, the daily timeseries of soil moisture in Fig. 4.2a indicates significant high frequency variability as well as a sharp decline from early May to August (Fig. 4.2a).

Similarly, the corresponding daily timeseries and the daily cumulative anomaly curves of precipitation and surface temperature areal averaged over 500 km centered over East Missouri are plotted in Figs. 4.2b and 4.3a, respectively. These plots yet again confirm that the steep decline in precipitation (Fig. 4.2b) and steep increase in temperature (Fig. 4.3a) over the period of the flash drought are more apparent in their respective daily accumulative anomaly curves than their daily timeseries. In Fig. 4.3b, the corresponding normalized cumulative anomaly curves of precipitation, soil moisture, temperature, and the drought index are plotted. The start and end of the flash drought period is marked by the steep decline in the cumulative anomaly curve of the drought index, which starts from 01 May 2012 and ends on 15 August 2012. It is interesting to note that the normalized daily cumulative anomaly curve of the drought index in Fig. 4.3b shows the flash drought period far more clearly than the remaining three other curves in the graph with its steep slope of -0.06 day^{-1}. Although the normalized daily cumulative anomaly curve of soil moisture and precipitation decline, and that of surface temperature increases over this diagnosed flash drought period, their slope is far more gradual than that of the drought index (Fig. 4.3b).

Figs. 4.4a, 4.4b, 4.5a, and 4.5b show the maps of the summation of the daily cumulative soil moisture, precipitation, and surface temperature anomalies and the corresponding drought index over the period of the diagnosed flash drought, which illustrates the spatial extent of the flash drought. The spatial patterns of the accumulated soil moisture anomalies over the flash drought period in Fig. 4.4a resemble to some extent the spatial pattern of the change in drought category from the USDM in Fig. 4.1a. This flash drought fingerprint is also apparent in the accumulated precipitation anomaly, which is negative, over a broad region around East Missouri (Fig. 4.4b). Similarly, the accumulated anomalies of temperature in Fig. 4.5a show that the

largest warming anomalies are stretched over a wide area around East Missouri. Finally, the spatial map of the cumulative anomalies of the drought index in Fig. 4.5b show uniformly, negative values across the US, except in the southeast and northwest region. However, the temporal correlations of the cumulative anomaly curve of the drought index with the corresponding timeseries in Fig. 4.3b indicate that a smaller subset of this region (shown by hatching) show a precipitous decrease in the drought index as in Fig. 4.3b. Therefore, the hatched region in Fig. 4.5b suggests the spatial extent of the flash drought of 2012, centered around East Missouri. It should be noted that the diagnosis of the flash drought from Fig. 4.3b is made from the normalized cumulative anomalies of soil moisture, precipitation, and surface temperature. These variables appear comparable, even though the summation of the normalized, daily cumulative soil moisture anomalies in Fig. 4.4a appear a couple of orders of magnitude smaller than those for the corresponding precipitation (Fig. 4.4b) and temperature (Fig. 4.5a) variables.

4.2 – South Iowa Flash Drought Verification

Four other separate cases of flash drought diagnosed by Otkin et al. (2013) and Christian et al. (2019) have been reviewed using the methodology proposed here. Fig. 4.6 shows the time series evolution of the cumulative anomaly curve of the drought index for 500 km radius centered around South Iowa, which detected a flash drought between 07 May 2012 to 15 August 2012. The normalized daily cumulative anomalies of soil moisture, precipitation, surface temperature, and drought index behave very similarly to those found in the East Missouri flash drought case (Fig. 4.6). The corresponding maps of the accumulated anomalies of soil moisture (Fig. 4.7a), precipitation (Fig. 4.7b), surface temperature (Fig. 4.8a), and the drought index (Fig. 4.8b) illustrate the spatial extent of the flash drought. The spatial extent of the negative daily

cumulative anomalies of soil moisture, precipitation, and drought index and the positive daily cumulative anomaly of surface temperature match up closely. This information paired with the fact that a flash drought was diagnosed in this region by the Otkin et al. (2013) and Christian et al. (2019) provides further evidence that a flash drought is taking place in South Iowa and that the event taking place over East Missouri is also a flash drought given this flash drought event over South Iowa overlaps with that of East Missouri and therefore the spatial maps shown in Figs. 4.4-4.5 and Figs. 4.7-4.8 appear very similar. The actual extent of the flash drought is given by the hatched region in Fig. 4.8b. The slope of the drought index in Fig. 4.8b is -0.06 day^{-1}, which is like that detected for East Missouri in Fig. 4.3b.

4.3 – Northeast Montana Flash Drought Verification

The next case of flash drought reviewed is over Northeast Montana (Fig. 4). Here, the gradient of the drought index over the flash drought period of 20 May 2017 to 03 August 2017 is -0.07 day^{-1}. Fig. 4.9 shows a slight increase in the daily cumulative anomaly of temperature paired with more significant decreases in the daily cumulative anomalies of soil moisture and precipitation. However, the daily cumulative anomaly of the drought index drops much more sharply during the period of the flash drought (Fig. 4.9). The spatial extent of the flash drought event indicated by the hatched area in Fig. 4.11b shows a similar decrease in the cumulative anomalies of soil moisture (Fig. 4.10a) and precipitation (Fig. 4.10b) and an increase in the cumulative anomalies of temperature (Fig. 4.11a). This flash drought is the same event that was discussed in the introduction located in the U.S. Northern Great Plains. Fig. 1.2 and Fig. 1.3 serve as complementary evidence that a flash drought is taking place at this location. The extent of this flash drought is not as wide as the East Missouri and South Iowa cases due to the more localized changes in anomalies.

4.4 – East Indiana Flash Drought Verification

Another flash drought event took place over East Indiana. This event started on 18 April 2007 and lasted until 01 July 2007. Normalized daily cumulative anomaly curves for this event show a similar temperature pattern to that seen in Northeast Montana, with slightly increasing cumulative temperature anomalies (Fig. 4.12). However, the cumulative anomaly curves for precipitation and soil moisture do not decrease by much over the flash drought period (Fig. 4.12). As a result, the cumulative anomaly curve for drought index does not drop as sharply over the flash drought period in this example (Fig. 4.12). The spatial extent of the soil moisture anomalies is confined from parts of the Southeast up to parts of the Midwest, and the cumulative anomalies are weakly negative (Fig. 4.13a). The spatial extent of the cumulative precipitation anomalies permeates throughout the East Coast and eastern parts of the Midwest, with negative signals showing up more strongly than for the soil moisture (Fig. 4.13b). The positive cumulative temperature anomalies show up more over northern states like Minnesota and Wisconsin, and also over Indiana, but not over the Southeast and the East Coast (Fig. 4.13b). The flash drought is centered over East Indiana due to the positive cumulative temperature anomalies coinciding with the negative precipitation and soil moisture anomalies (Fig. 4.14a). The spatial extent of the negative cumulative anomalies of the drought index and the hatching location also confirm this flash drought location (Fig. 4.14b).

4.5– South Central Georgia Flash Drought Verification

The final flash drought event analyzed is over South Central Georgia from 03 October 2016 to 27 November 2016). The normalized daily cumulative anomaly curves show a slight increase for temperature, a significant decrease in soil moisture and precipitation, and a sharp decrease in the drought index (Fig. 4.15). The spatial extent of the negative soil moisture and

precipitation cumulative anomalies are confined to the Southeast US while the positive temperature cumulative anomalies are most prevalent in the Central US and parts of the Southeastern US (Figs. 4.16a, 4.16b, 4.17a). The drought index spatial extent is a bit more sporadic, however there are negative cumulative anomalies in the southeast (Fig. 4.17b). South Central Georgia is in the transition zone between positive and negative anomalies for soil moisture, precipitation, and temperature and falls on the edge of the drought index hatch. However, our cumulative anomaly curves indicate that there is a flash drought taking place in this region. Since these curves look at each variable at a 500 km radius around South Central Georgia, it suggests that the center of the flash drought is not in South Central Georgia like is suggested by Otkin et al. (2013) and Christian et al. (2019) but further to the northwest instead.

The slope of the drought index line fell in between -0.05 day^{-1} and -0.07 day^{-1} during the flash drought period for all the cases. This range of slopes will be used to in the next section to identify landfalling Atlantic TCs that are inducing flash droughts in their wake. Following landfall, if there is a drop off in the slope of the drought index line between -0.05 day^{-1} and -0.07 day^{-1}, then a flash drought will have taken place according to our drought index.

4.6 – Summary

In this chapter we have verified the drought index with five previously documented cases of flash drought based on the USDM and other academic studies. In each of these case studies, our objective drought index identifies the evolving flash drought over the period that matches with the USDM and previous academic studies diagnoses. Furthermore, the spatial extent of the flash drought reasonably matches up with the USDM maps during this timeframe. There are, however, subtle differences that stem from the vastly different methodologies of the USDM and our drought index. The differences in the datasets used in the methodologies of the USDM and

our drought index also manifest themselves as differences in the results, Nonetheless, the five illustrations of flash drought detection indicate the efficacy of the drought index in diagnosing flash droughts in the continental US. With the confidence in the drought index now realized, we will proceed to investigate the incidence of flash droughts in the wake of landfalling Atlantic TCs in the next chapter.

5. RESULTS: FLASH DROUGHTS IN THE WAKE OF LANDFALLING ATLANTIC TROPICAL CYCLONES

5.1 - Flash Drought Events Associated with Landfalling Tropical Cyclones

After examining all landfalling Atlantic TC's in the continental US from 2000-2018, four distinct events were identified that produced flash droughts post-landfall. Therefore, unlike the Maritime Continent region, the incidence of flash droughts from landfalling Atlantic TCs is fairly uncommon, given that only four out of 30 cases (~13%) exhibited flash droughts post-landfall. As in the previous flash drought case analysis, a timeseries of all three variables (soil moisture, precipitation, and surface temperature) and the drought index averaged around a radius of 500 km from the point of landfall is plotted in Figs. 4.18 and 4.19 for these four cases of landfalling TCs. The start and end date of the flash drought are indicated in the timeseries of the drought index for all cases (Figs. 4.18 and 4.19). The slope of the drought index computed over the period of the flash drought for Hurricane Humberto is -0.06 day^{-1} (Fig. 4.18a); Hurricane Isaac is -0.07 day^{-1} (Fig. 4.18b); Hurricane Matthew is -0.09 day^{-1} (Fig. 4.19a); and Harvey is -0.05 day^{-1} (Fig. 4.19b). These slopes are comparable to the previous cases discussed in Section 3a.

5.1a – Hurricane Humberto

Humberto became a hurricane (with ~80 kt surface winds) when located about 20 n mi south of High Island, Texas around 0400 UTC 13 September 2007, qualifying it as one of the most rapidly intensifying North Atlantic TCs (Brennan et al. 2007). After landfall, the hurricane translated northeastward toward southwestern Louisiana and became a tropical depression near Alexandria, Louisiana (late on 13 September) before dissipating over Central Mississippi (Fig. 4.20a). The flash drought was first diagnosed on 30 September (Fig. 4.20a), over two weeks after

the TC had dissipated. However, this flash drought is determined to be associated with the landfall of Humberto because the decline in precipitation, the rise in surface temperature, and the gradual decrease in soil moisture in the wake of the hurricane contributed to the onset of this flash drought, which ended on 10 December (Fig. 4.18a).

5.1b Hurricane Isaac

Hurricane Isaac made the first landfall at Southwest Pass, Louisiana around 0000 UTC 29 August 2012 with maximum sustained winds of 70 kt. The center of the hurricane wobbled westward back over water and made a second landfall at Port Fourchon, Louisiana around 0800 UTC 29 August (Berg 2013). After landfall, the storm gradually weakened to a tropical depression by 0000 UTC 31 August as it moved northwestward across Louisiana and then over southern Arkansas (Fig. 8b). The depression finally dissipated around 0600 UTC on 1 September when west-southwest of Jefferson City, Missouri (Fig. 4.20b). The remnants of Isaac produced several tornados across the Mississippi River Valley on 1 September as it veered northeastward and eastward across Missouri and Illinois. The onset of the flash drought associated with Isaac was diagnosed as 5 September, five days after landfall (Fig. 4.18b). The precipitous decrease in rainfall and soil moisture after landfall led to the onset of the flash drought. The increase in surface temperature, however, occurred far later, which led to a further increase in the severity of the flash drought that ends on 15 November (Fig. 4.18b).

5.1c – Hurricane Matthew

Matthew was an especially deadly hurricane that made multiple landfalls as a Category 5 hurricane along the coasts of Haiti, Cuba, Grand Bahama Island and then as a Category 1 hurricane along the central coast of South Carolina (Stewart 2017). Hurricane Matthew accounted for 585 direct deaths: 546 in Haiti, 34 in the US, 4 in the Dominican Republic, and 1

in St. Vincent and the Grenadines (Stewart 2017). Hurricane Matthew remained about 30 n mi offshore of the Florida Atlantic coast, as a Category 2 hurricane with its winds impacting Cape Canaveral, Vero Beach, and Jacksonville Beach in Florida by 0000 UTC 8 October 2016 (Fig. 4.21a). Hurricane Matthew continued to move northward toward South Carolina making landfall at 1500 UTC on 8 October at Cape Romain National Wildlife Refuge (Fig. 4.21a). As a result of the storm's large hurricane force wind field and its track along the eastern coast of the southeastern United States, there was significant inundation from storm surge along the coasts and well inland of the coasts of Florida, Georgia, and South Carolina (Stewart 2017). The diagnosis of the onset of flash drought occurred on 10 October (Fig. 4.19a), two days after Matthew skirted the coast of Florida. As in the previous cases, the decrease in precipitation and soil moisture and gradual increase in surface temperature in the wake of storm passage near Flagler, Florida led to the onset of the flash drought, manifested by the sharp decline of the drought index (Fig. 4.19a).

5.1d – Hurricane Harvey

Hurricane Harvey made landfall in Texas mainland as a Category 4 hurricane at 0600 UTC 26 August 2017 along the coast of Copano Bay as a Category 4 hurricane. It rapidly weakened to tropical storm status within 12 hours of landfall (Blake and Zelinsky 2018). However, Harvey remained nearly stationary, with its center over or near the Texas coast for four days before making its final landfall over Southwestern Louisiana near Cameron at 0800 UTC 30 August (Fig. 4.21b). During this four day period, the storm produced over 60 in. of rainfall over the southeastern coast of Texas, causing catastrophic flooding. The onset of the flash drought occurred soon after on 1 September and lasted until 1 November (Fig. 4.19b). This

period of flash drought was characterized by a gradual increase in surface temperature, decline in precipitation, and a gradual decrease in soil moisture.

5.1e – Analyzing Tropical Cyclone Induced Flash Drought

The corresponding spatial patterns of these flash droughts as represented by the accumulated normalized values of the drought index over the period of the diagnosed flash drought are shown in Figs. 4.20 and 4.21. These cases reveal that the flash drought as associated with TC landfall is part of a larger scale drought that stretches far beyond the point of landfall. The wake of the landfalling TC leaves behind favorable conditions for a flash drought to expand the already existing drought to the path of the TC. The desiccation of moisture from the atmospheric column and the associated subsidence in the wake of the landfalling TC exacerbated and accelerated the advancing drought over the landfalling region. For example, in the case of Humberto, the flash drought identified near Galveston, Texas can be viewed as an extension of the drought that stretches across the southern US and into the mid-Atlantic States, albeit not all the spatial extent of the drought necessarily evolved as a flash drought (Fig. 4.20a). Similarly, the flash drought identified in association with Hurricane Isaac also extends along the Texas and Louisiana coasts, which could be associated with the drought across the western and mid-western US (Fig. 4.20b). Likewise, in the cases of Hurricanes Matthew and Harvey, the flash droughts at the point of landfall occur in conjunction with more widespread droughts across the southeastern (Fig. 4.21a) and midwestern US (Fig. 4.21b), respectively.

In each of these four landfalling TCs, the soil moisture during the period of the flash drought is not excessively anomalous at the point of landfall (Figs. 4.22 and 4.23). The summation of the normalized, daily cumulative anomalies of soil moisture over the diagnosed flash drought period around the landfall point in all four cases are greater than zero, suggesting

that the soil was anomalously wet, albeit slightly (Figs. 4.22 and 4.23). This would seem somewhat obvious given the amount of rainfall resulting from the TCs and associated storm surge that would have moistened the soil. However, the corresponding summation of the normalized, daily cumulative anomalies of precipitation over the period of the flash drought around the landfall point are well below zero (Figs. 4.24 and 4.25). In fact, the dry anomalies in Figs. 4.24 and 4.25 nearly track the TC after landfall in all four cases. Similarly, the summation of the normalized, cumulative surface temperatures over the period of the flash drought are positive in all four cases (Figs. 4.26 and 4.27). These figures suggest that the lack of precipitation and the warming surface temperature in the wake of these landfalling TC's leads to the diagnosed flash drought.

5.2 – Landfalling Tropical Cyclones Not Associated with Flash Drought

Due to the small number of landfalling Atlantic TCs causing flash droughts, it is important to review some of the hurricanes that were analyzed but did not induce a flash drought. The hurricanes that will be discussed are Hurricane Katrina, Hurricane Rita, and Hurricane Ike. These three storms will be discussed because they exhibited a variety of drought index behaviors following landfall. They either showed a less steep decrease in the drought index values, an increase in the drought index values, or a steep decrease in drought index values long after landfall.

5.2a – Hurricane Katrina Drought Index Analysis

Hurricane Katrina made its first landfall in South Florida on 25 August 2005 and would eventually make a second landfall near Buras, Louisiana on 29 August 2005 as a Category 3 Hurricane with maximum sustained winds of 110 kt (Knabb et al. 2005). Katrina made another landfall near the Louisiana/Mississippi border with an intensity near 105 kt. Katrina then

weakened and eventually dissipated as it moved its way toward the Great Lakes (Knabb et al. 2005). The rainfall that resulted from Hurricane Katrina over Buras, Louisiana, and the surrounding 500 km radius, did not cause a major change in the normalized daily cumulative precipitation anomaly (Fig. 4.28). The normalized daily cumulative temperature anomaly shows a slight positive trend, while the normalized daily cumulative soil moisture and precipitation anomalies exhibit a slight negative trend over time (Fig. 4.28). This results in a drought index with a cumulative anomaly that steadily decreases over the 12 weeks following hurricane landfall, with a slope of about -0.03 day^{-1}, but not quickly enough to result in a flash drought (Fig. 4.28).

5.2b – Hurricane Rita Drought Index Analysis

Hurricane Rita made landfall as a Category 3 Hurricane before making landfall at 0740 UTC on 24 September 2005 with an estimated intensity of 100 kt just west of Johnson's Bayou, Louisiana (Knabb et al. 2005). Rita quickly weakened as it moved northward into Arkansas and eventually dissipated over Illinois after it merged with a frontal system on 26 September (Knabb et al. 2005). The normalized daily cumulative anomalies for Hurricane Rita look very similar to those from Hurricane Katrina, which is not surprising since they both made landfall within a month of one another on opposite sides of Louisiana (Fig. 4.29). Slight positive cumulative temperature anomaly trends are paired with slight negative cumulative soil moisture and precipitation trends to create a cumulative anomaly of drought index that steadily decreases over the 12 weeks following landfall, with a slope of about -0.03 day^{-1}, but not at a fast enough rate to induce a flash drought.

5.2c – Hurricane Ike Drought Index Analysis

Hurricane Ike is the final hurricane that will be analyzed. Throughout its lifecycle, Hurricane Ike made landfall in the Bahamas, Cuba, and eventually Texas. The landfall in Texas took place at Galveston Island, Texas at 0700 UTC 13 September 2008 with maximum winds of 95 kt (Berg 2008). After landfall, Ike quickly weakened as it moved across Texas, Arkansas, Missouri, and into the Ohio Valley while interacting with a front and becoming extratropical (Berg 2008). Ike eventually dissipated over Canada on 15 September (Berg 2008). There was an initial spike in the normalized cumulative anomalies of the drought index, soil moisture, and precipitation associated with landfall (Fig. 4.30). These anomalies, along with the cumulative temperature anomalies, slowly decreased over the next couple of months (Fig. 4.30). Around the beginning of December, the cumulative anomalies of temperature begin to increase associated with a sharp decrease in the drought index cumulative anomalies (Fig. 4.30). This decrease in the drought index could be a signal for a flash drought; however, it occurs too far after Ike's landfall to be associated with the hurricane. The slope of the drought index over the 12-week period following hurricane landfall is -0.015 day^{-1}.

These are just 3 of the 27 TCs that did not induce flash droughts after landfall according to our drought index, meaning that Atlantic TC-induced flash droughts are a comparatively rare event, at least in the past two decades.

6. CONCLUSION

This thesis describes and evaluates a new and relatively simple drought index that can be diagnosed from daily values of soil moisture, surface temperature, and precipitation. Flash drought is a relatively newly defined term that can be used to diagnose climate anomalies. However, the lack of data prevents the ability to look too far in the past to diagnose a flash drought. One of the advantages of the methodology is that one can objectively define the start and end of the flash drought period by the rate of change of the drought index. The drought index is also based on observed variables instead of modeled ones. This allows it to be used to detect and forecast flash droughts in real-time situations using a simplified methodology. Past methodologies relied on subjective analyses or sophisticated land surface models to detect and forecast flash drought events. As a result, there was a need for a new kind of flash drought detection method.

The efficacy of diagnosing flash drought from the new index is demonstrated with five known cases of flash drought from the USDM and other previous studies. The East Missouri Flash Drought took place from 01 May 2012 to 15 August 2012, and the impacts were centered on the Midwest. The South Iowa Flash Drought was part of the same event as the East Missouri Flash Drought and lasted from 07 May 2012 to 15 August 2012. The impact of this flash drought was limited to the Midwest. The Northeast Montana Flash Drought occurred from 20 May 2017 to 03 August 2017, and its impacts were limited to the Northern US. The East Indiana Flash Drought began on 18 April 2007 and ended on 01 July 2007 with impacts felt in the Eastern Midwest and Eastern United States. The final flash drought case analyzed was the South Central Georgia Flash Drought from 03 October 2016 to 27 November 2016 which impacted the Southeast US. The drought index detected all these flash drought events that were proven to have

occurred by previous studies. The ability of the drought index to detect these events within the timeframe that they took place without failure provides confidence in its ability to detect a flash drought in the wake of a landfalling Atlantic TC.

Four cases of landfalling Atlantic TCs along the US Atlantic and Gulf Coasts that were associated with flash droughts in their wake were identified. The four landfalling tropical cyclones were Hurricanes Humberto, Isaac, Matthew, and Harvey. In three of these cases, the flash drought was initiated within a few days of landfall, while in the case of Hurricane Isaac it began two weeks after landfall. In all cases, the flash drought that started at the point of the landfall was coincident with a more widespread drought over a larger area, suggesting that the conditions in the wake of the landfalling TC exacerbated and accelerated the flash drought conditions. The analysis of these flash drought events suggests that negative (dry) precipitation and positive (warm) surface temperatures in the wake of the landfalling TC are principal causes of the droughts while the soil moisture anomalies are weakly positive (wet). The fact that this study was able to isolate only four cases of flash drought out of 30 cases of Atlantic TC landfalls in the US suggests that such events are relatively uncommon in the wake of Atlantic TC landfalls. Due to the small sample size, the link between flash droughts and landfalling Atlantic TC cannot be dismissed.

Three TCs that did not result in flash drought were analyzed more closely: Hurricanes Katrina, Rita, and Ike. These hurricanes differed from the hurricanes that caused flash drought because following landfall they either exhibited a less steep decrease in the drought index values, showed an increase in the drought index, or showed a steep decrease in drought index values after a significant amount of time had taken place after landfall.

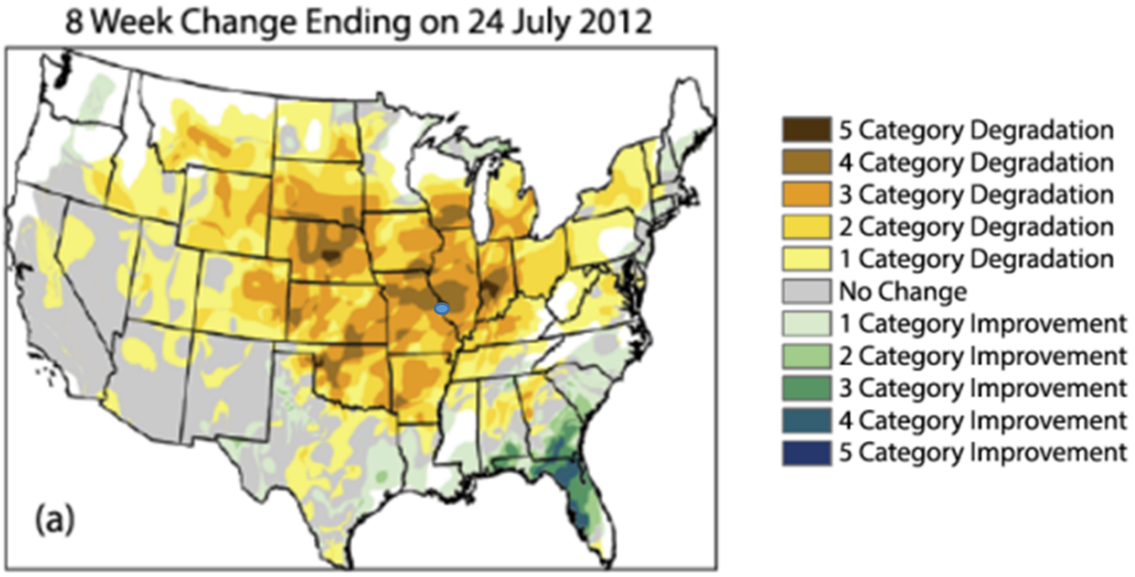

Figure 4.1: a) The case of a flash drought centered around East Missouri (shown by the blue dot), showing the 8-week change in the USDM drought category ending on 24 July 2012 (after Otkin et al. 2018).

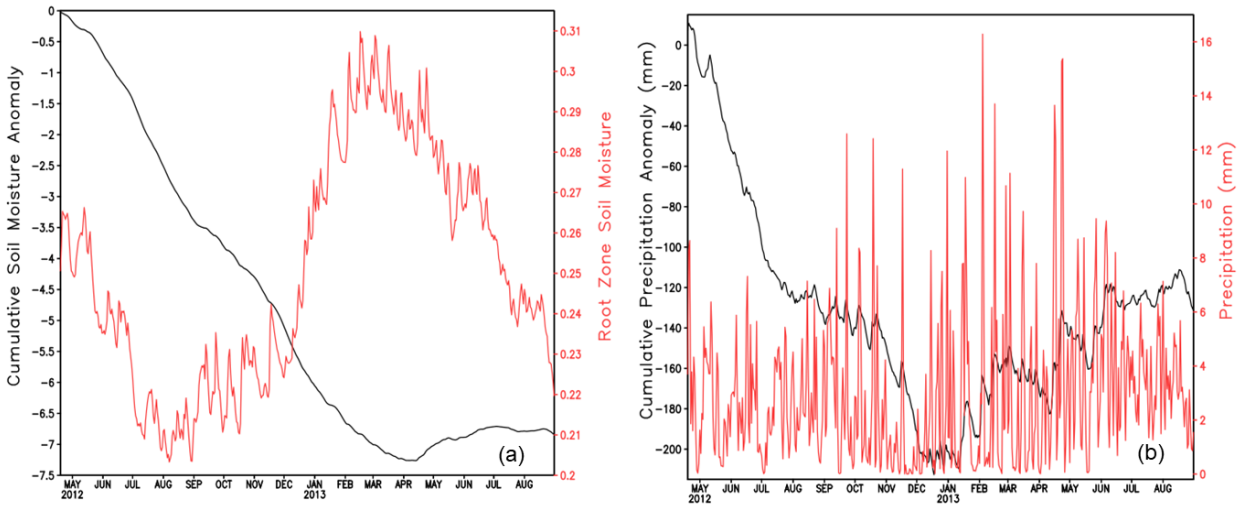

Figure 4.2: The corresponding area averaged time series at 500 km radius centered over East Missouri of daily a) cumulative soil moisture anomaly (black line) and soil moisture (red line), b) cumulative precipitation anomaly (mm; black line) and precipitation (mm day^{-1}; red line).

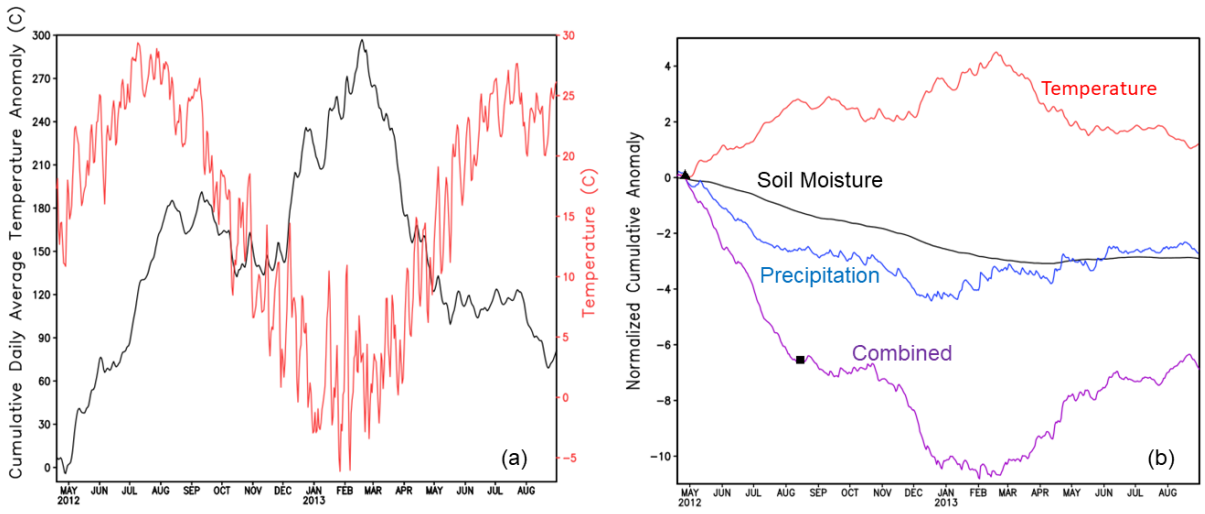

Figure 4.3: The corresponding area averaged time series at 500 km radius centered over East Missouri of daily a) cumulative surface temperature anomaly (black line) and surface temperature (°C; red line). b) The corresponding normalized daily cumulative anomalies of temperature, soil moisture, precipitation, and the drought index (see text) curves. The start and end of the flash drought as diagnosed from the cumulative anomaly curve of the drought index in Fig. 4.3b are marked by the black solid triangle (01 May 2012) and square (15 August 2012), respectively. The gradient of the drought index over the flash drought period from (e) is 0.06 day^{-1}.

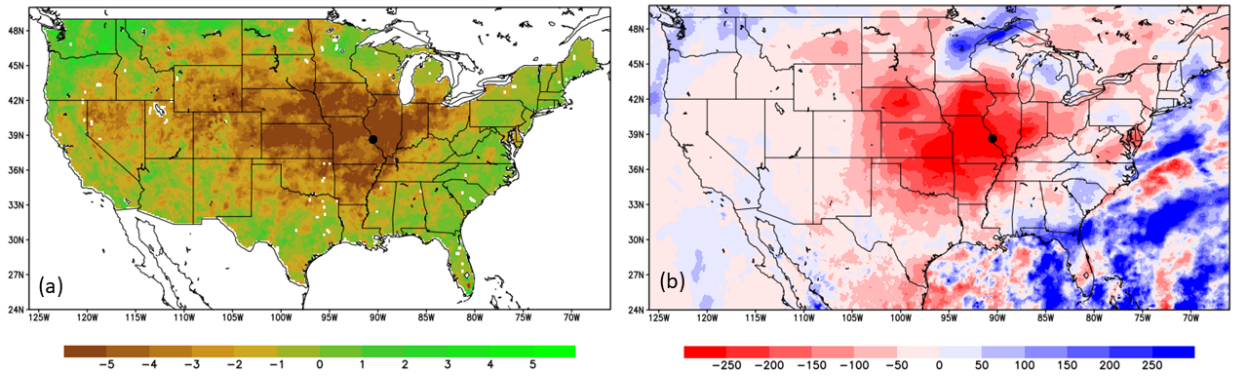

Figure 4.4: The map of the daily cumulative a) soil moisture and b) precipitation for the flash drought event centered over East Missouri in 2012 (see Fig. 4.1a). The daily anomalies are summed over the period of the flash drought diagnosed in Fig. 4.3b. The black dot in each of the panels indicate the location of East Missouri.

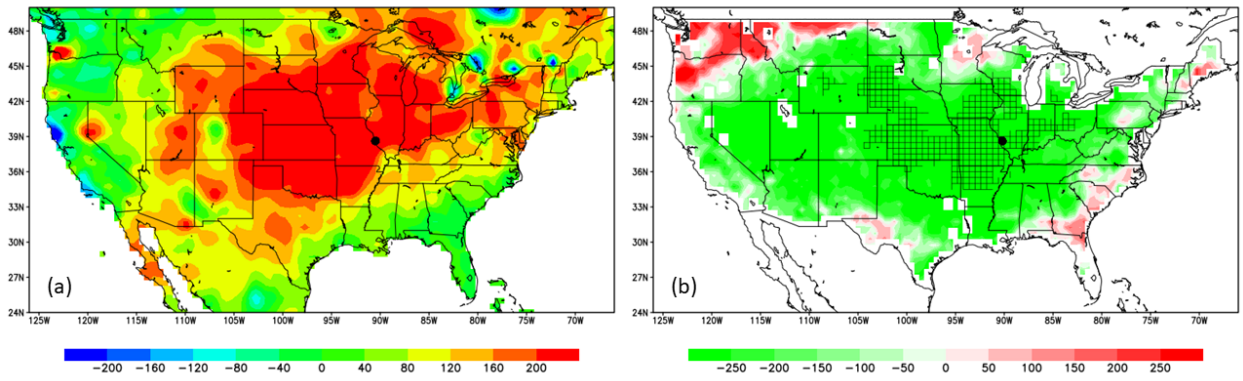

Figure 4.5: The map of the daily cumulative a) surface temperature and b) the drought index variable for the flash drought event centered over East Missouri in 2012 (see Fig. 4.1a). The daily anomalies are summed over the period of the flash drought diagnosed in Fig 4.3b. The hatching in (b) indicates significant correlation (at 1% significance level) of the evolution of the combined normalized variable with its corresponding evolution over a 500 km radius region around East Missouri indicated in Fig. (4.3b). The black dot in each of the panels indicate the location of East Missouri.

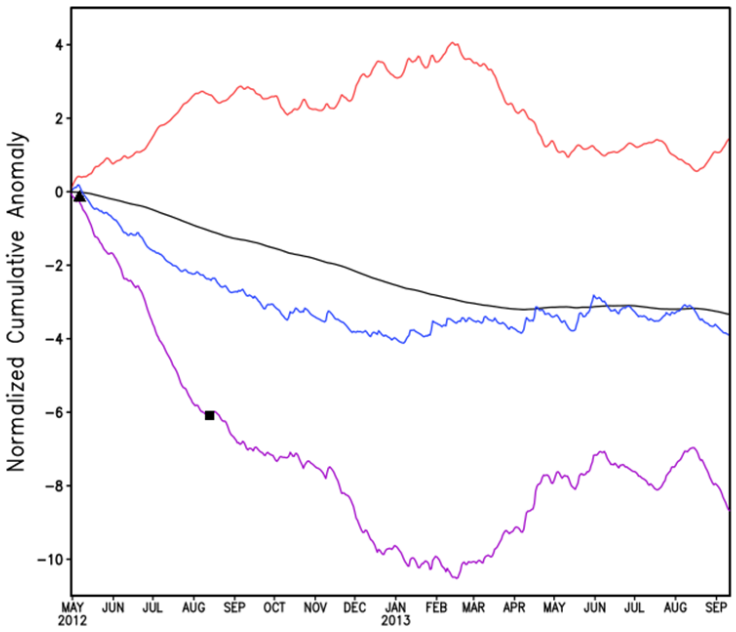

Figure 4.6: Normalized daily cumulative anomaly curves of temperature, soil moisture, precipitation, and the drought index computed over an area of 500 km radius centered around South Iowa. The start (07 May 2012) and end (15 August 2012) of the flash drought period is indicated by a triangle and a square, respectively. The gradient of the drought index over the flash drought period is 0.06 day^{-1}.

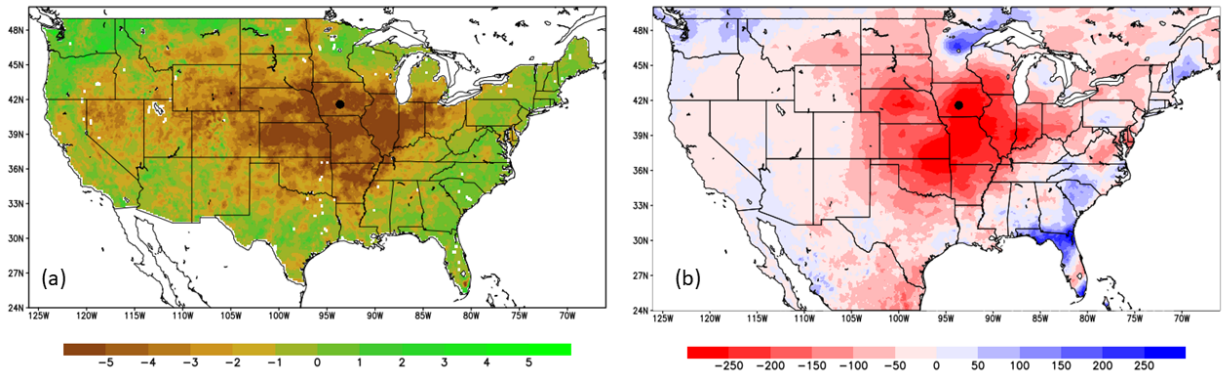

Figure 4.7: The corresponding cumulative a) soil moisture and b) precipitation anomalies over the period of the diagnosed flash drought from Fig. 4.6 with the black dot marking South Iowa.

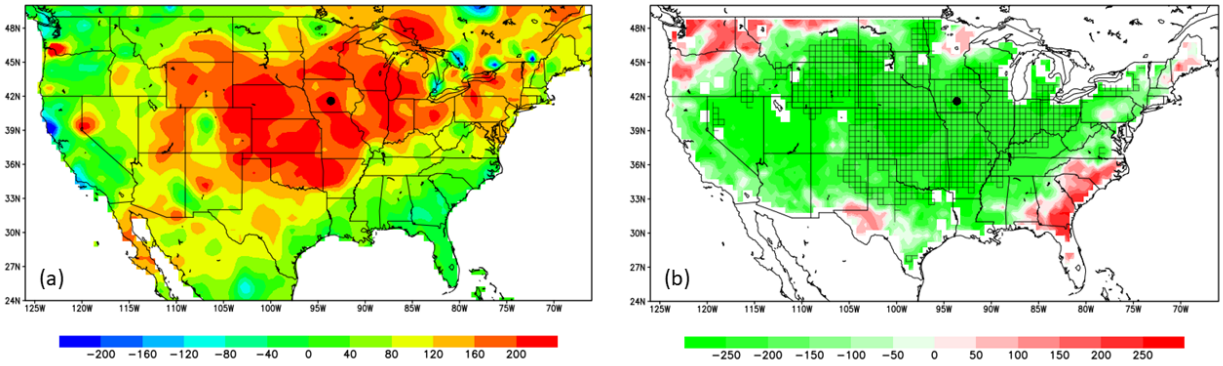

Figure 4.8: The corresponding cumulative a) surface temperature and b) drought index anomalies over the period of the diagnosed flash drought from Fig. 4.6 with the black dot marking South Iowa. The hatching in (b) indicates significant correlation (at 1% significance level) of the evolution of the drought index with its corresponding evolution over a 500 km radius region around South Iowa indicated in Fig. 4.6.

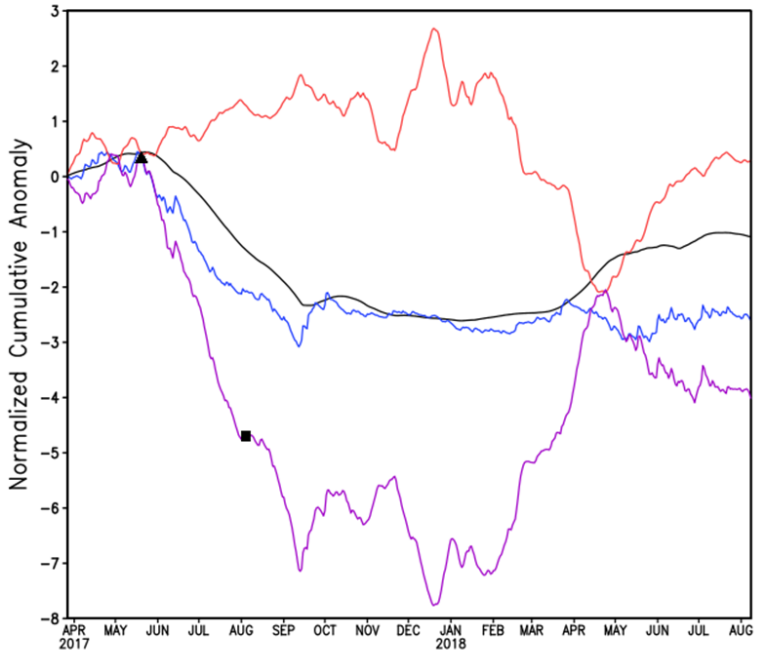

Figure 4.9: Normalized daily cumulative anomaly curves of temperature, soil moisture, precipitation, and the drought index computed over an area of 500 km radius centered around Northeast Montana. The start (20 May 2017) and end (03 August 2017) of the flash drought period is indicated by a triangle and a square, respectively. The gradient of the drought index over the flash drought period is 0.07 day^{-1}.

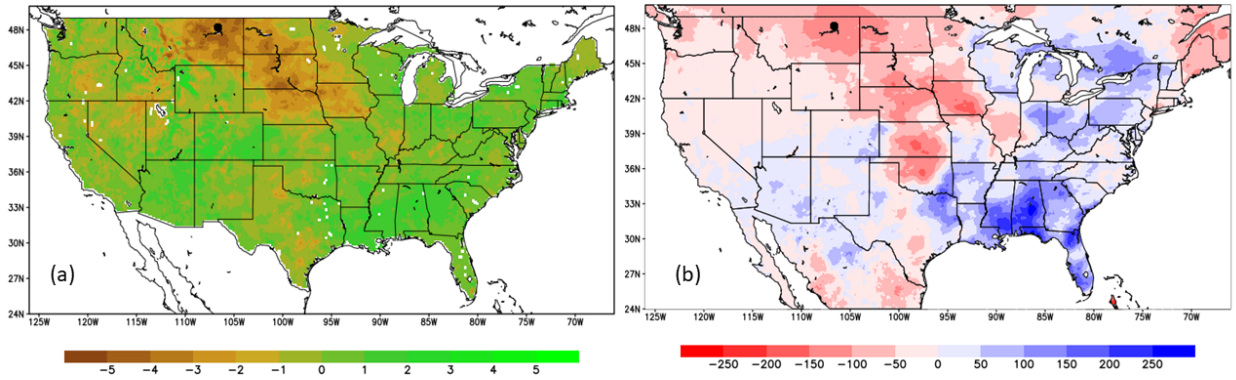

Figure 4.10: The corresponding cumulative a) soil moisture and b) precipitation anomalies over the period of the diagnosed flash drought from Fig. 4.9 with the black dot marking Northeast Montana.

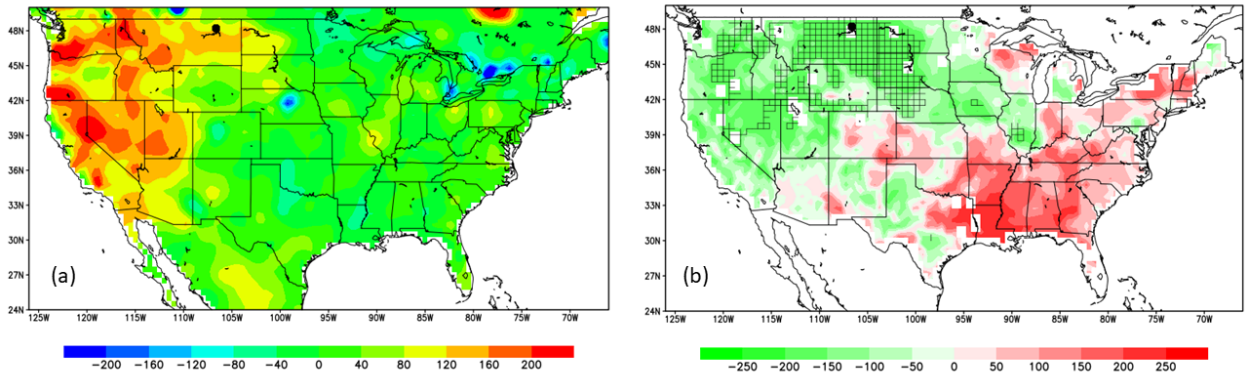

Figure 4.11: The corresponding cumulative a) surface temperature and b) drought index anomalies over the period of the diagnosed flash drought from Fig. 4.9 with the black dot marking Northeast Montana. The hatching in (b) indicates significant correlation (at 1% significance level) of the evolution of the drought index with its corresponding evolution over a 500 km radius region around Northeast Montana indicated in Fig. 4.9.

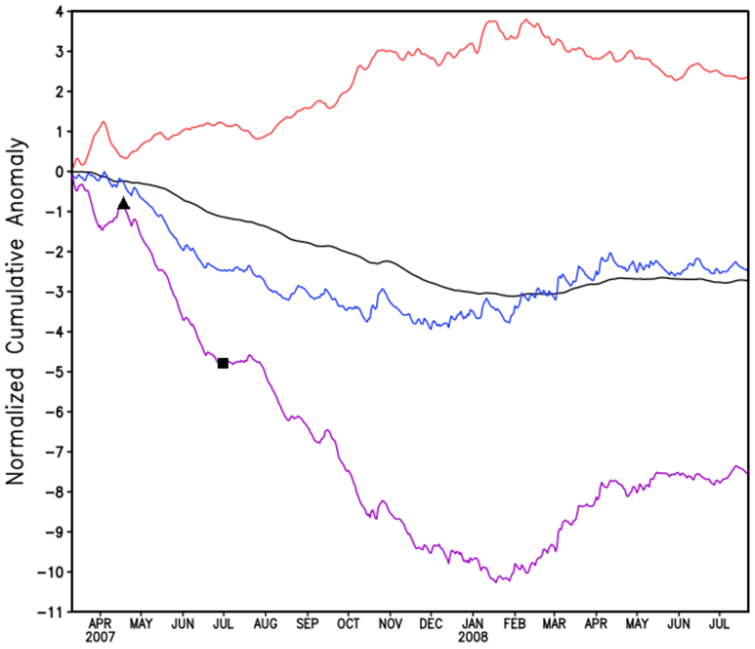

Figure 4.12: Normalized daily cumulative anomaly curves of temperature, soil moisture, precipitation, and the drought index computed over an area of 500 km radius centered around East Indiana. The start (18 April 2007) and end (01 July 2007) of the flash drought period is indicated by a triangle and a square, respectively. The gradient of the drought index over the flash drought period is 0.05 day^{-1}.

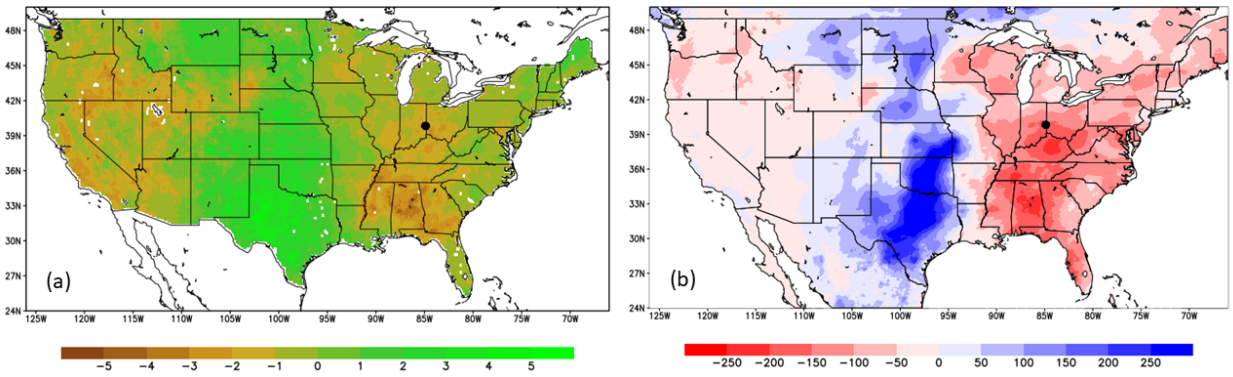

Figure 4.13: The corresponding cumulative a) soil moisture and b) precipitation anomalies over the period of the diagnosed flash drought from Fig. 4.12 with the black dot marking East Indiana.

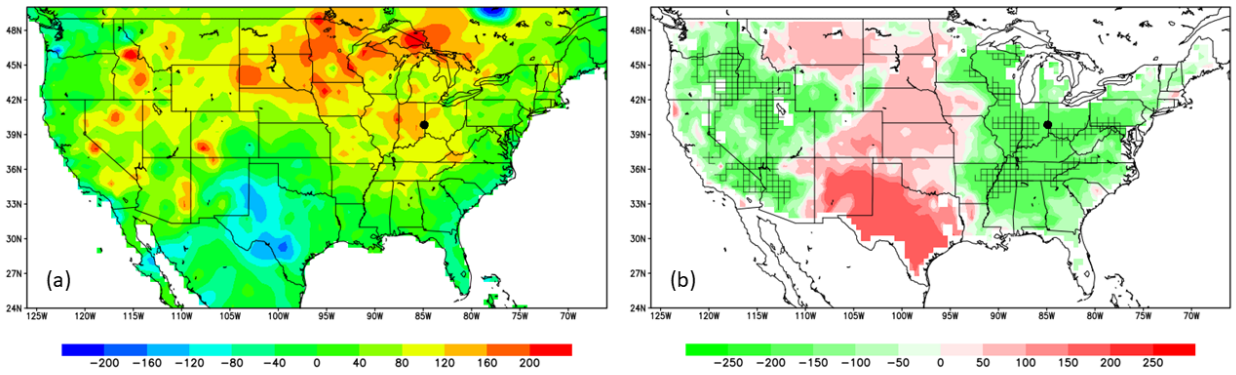

Figure 4.14: The corresponding cumulative a) surface temperature and b) drought index anomalies over the period of the diagnosed flash drought from Fig. 4.12 with the black dot marking East Indiana. The hatching in (b) indicates significant correlation (at 1% significance level) of the evolution of the drought index with its corresponding evolution over a 500 km radius region around East Indiana indicated in Fig. 4.12.

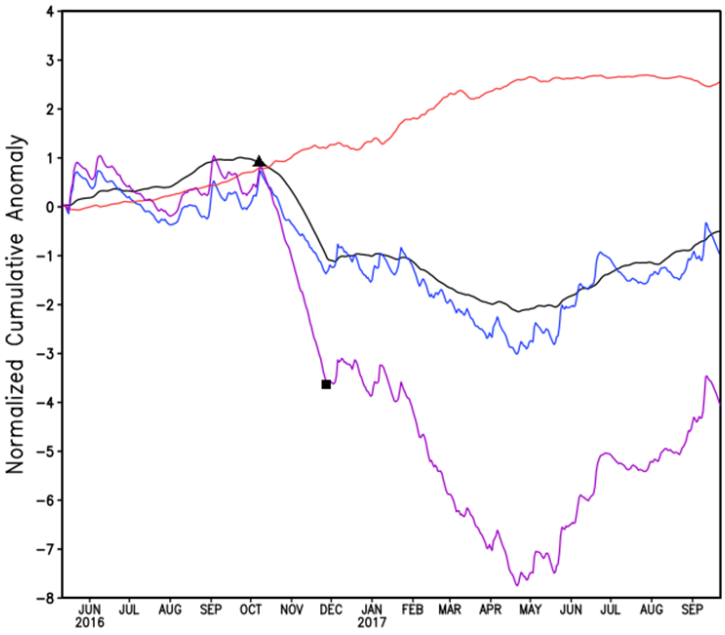

Figure 4.15: Normalized daily cumulative anomaly curves of temperature, soil moisture, precipitation, and the drought index computed over an area of 500 km radius centered around South Central Georgia. The start (03 October 2016) and end (27 November 2016) of the flash drought period is indicated by a triangle and a square, respectively. The gradient of the drought index over the flash drought period is 0.07 day^{-1}.

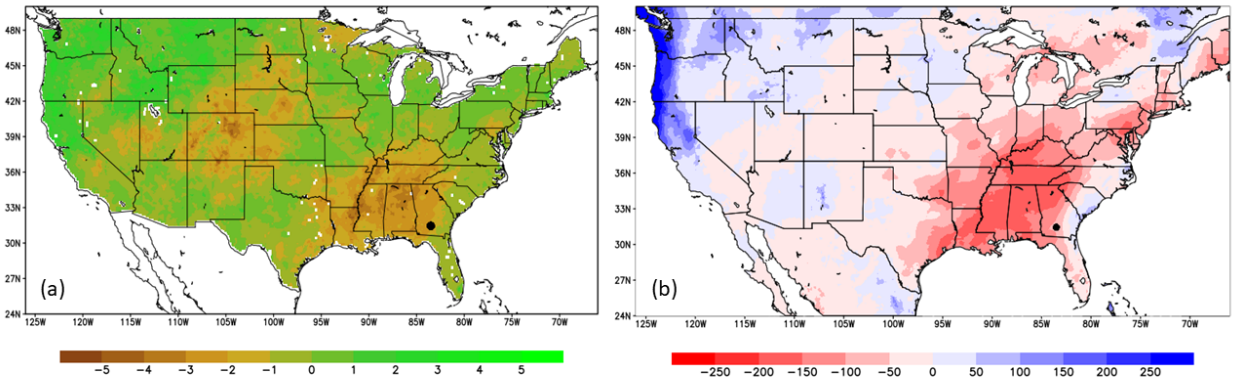

Figure 4.16: The corresponding cumulative a) soil moisture and b) precipitation anomalies over the period of the diagnosed flash drought from Fig. 4.15 with the black dot marking South Central Georgia.

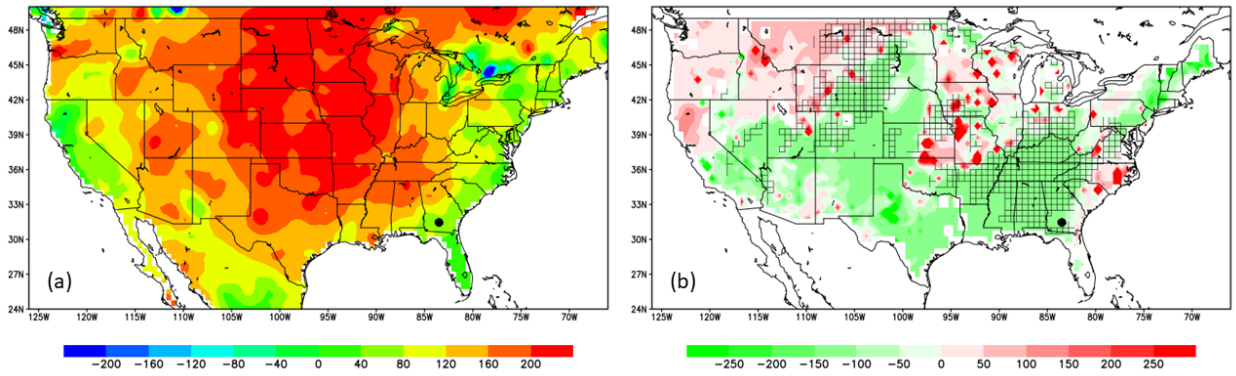

Figure 4.17: The corresponding cumulative a) surface temperature and b) drought index anomalies over the period of the diagnosed flash drought from Fig. 4.15 with the black dot marking South Central Georgia. The hatching in (b) indicates significant correlation (at 1% significance level) of the evolution of the drought index with its corresponding evolution over a 500 km radius region around South Central Georgia indicated in Fig. 4.15.

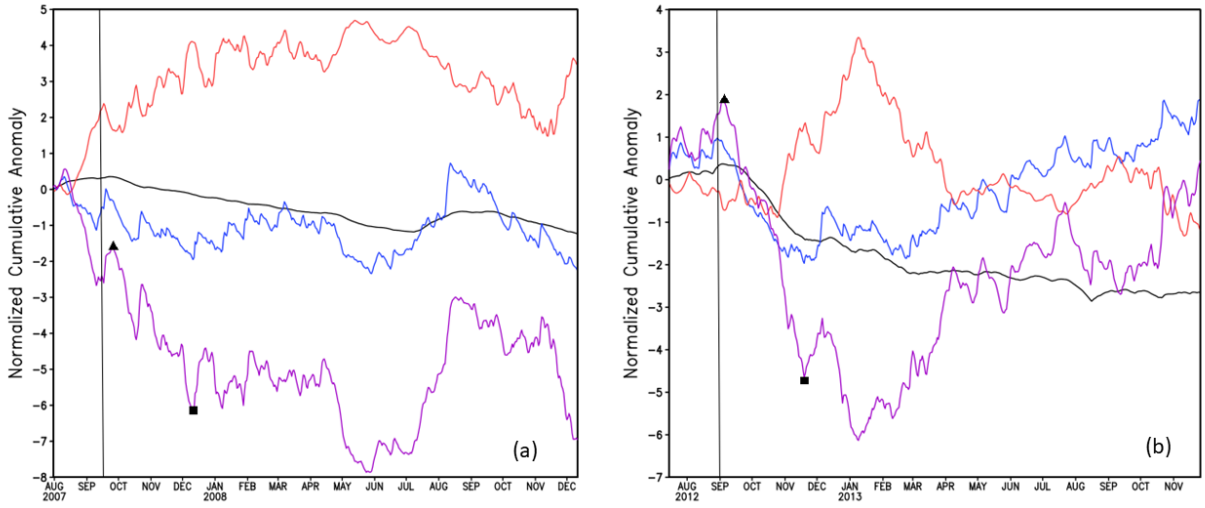

Figure 4.18: The area averaged time series of the normalized cumulative anomalies of daily soil moisture (black line), precipitation (blue line), surface temperature (red line), and drought index (purple line) for the landfalling case of a) Hurricane Humberto of 2007 and b) Hurricane Isaac of 2012. The area average of the time series is conducted over a radius of 500 km from the point of landfall as the center. The location of the landfall of the hurricane is indicated in Fig. 4.20. The start and end of the flash drought as diagnosed from the cumulative anomaly curve of the drought index in are marked by the black solid triangle and square, respectively.

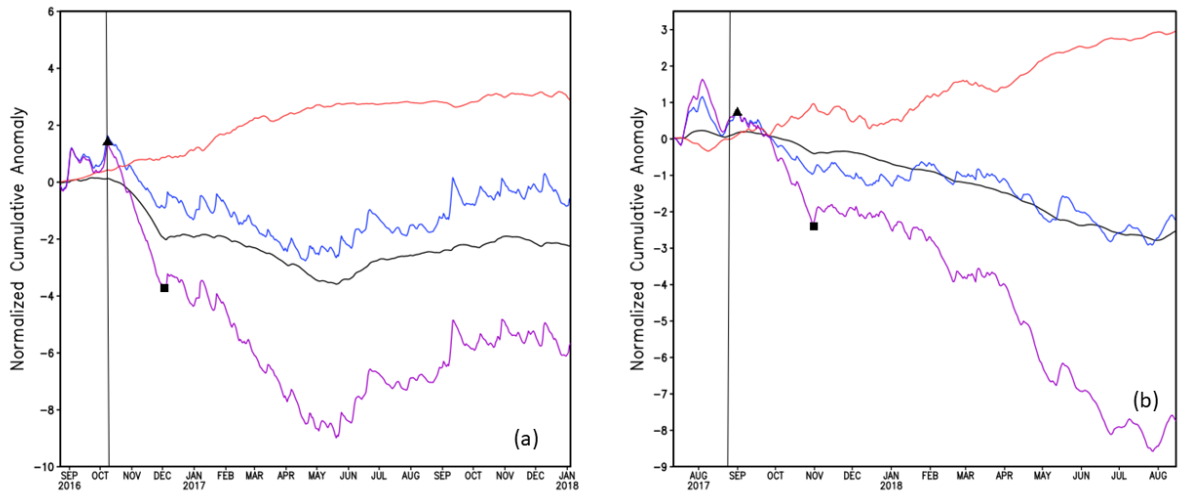

Figure 4.19: The area averaged time series of the normalized cumulative anomalies of daily soil moisture (black line), precipitation (blue line), surface temperature (red line), and drought index (purple line) for the landfalling case of a) Hurricane Matthew of 2016 and b) Hurricane Harvey of 2017. The area average of the time series is conducted over a radius of 500 km from the point of landfall as the center. The location of the landfall of the hurricane is indicated in Fig. 4.21. The start and end of the flash drought as diagnosed from the cumulative anomaly curve of the drought index in are marked by the black solid triangle and square, respectively.

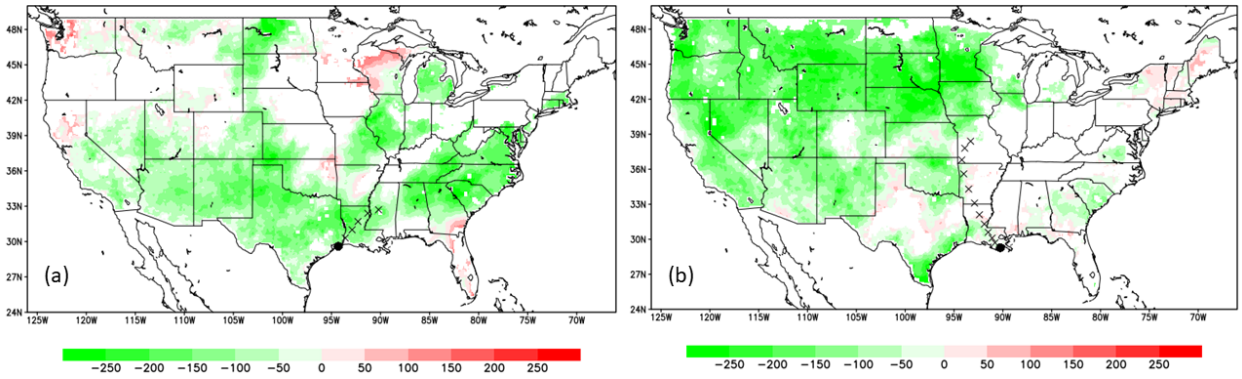

Figure 4.20: The map of the normalized, daily cumulative anomalies of the drought index for the flash drought events associated with the landfall of Hurricanes a) Humberto of 2007 and b) Isaac of 2012. The daily normalized anomalies of the drought index are summed over the period of the flash drought as indicated in Fig. 4.18. The black dot in each of the panels indicate the location of the landfall of the hurricane. The cross marks indicate the track of the hurricane after its landfall at 6-hour interval from the best track. All shaded values indicate significant correlation with the evolution of the drought index around an area of 500 km radius from the point of landfall of the hurricane at 95% confidence interval according to t-test.

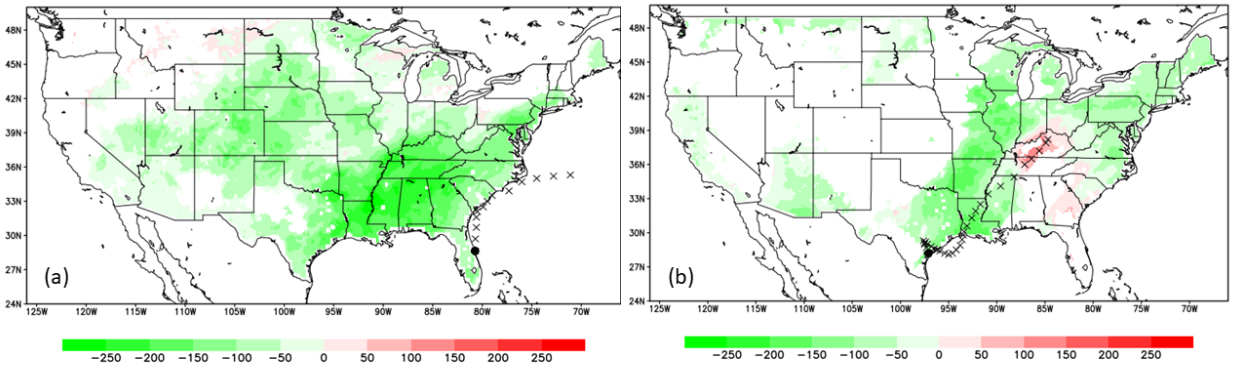

Figure 4.21: The map of the normalized, daily cumulative anomalies of the drought index for the flash drought events associated with the landfall of Hurricanes a) Matthew of 2016 and b) Harvey of 2017. The daily normalized anomalies of the drought index are summed over the period of the flash drought as indicated in Fig. 4.19. The black dot in each of the panels indicate the location of the landfall of the hurricane. The cross marks indicate the track of the hurricane after its landfall at 6-h interval from the best track. All shaded values indicate significant correlation with the evolution of the drought index around an area of 500 km radius from the point of landfall of the hurricane at 95% confidence interval according to t-test.

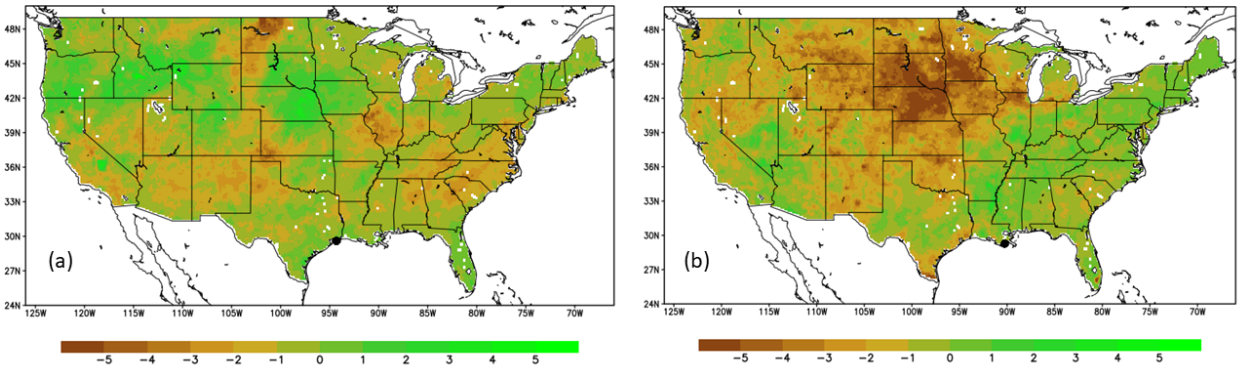

Figure 4.22: The map of the normalized, daily cumulative anomalies of the soil moisture for the flash drought events associated with the landfall of Hurricanes a) Humberto of 2007 and b) Isaac of 2012. The daily normalized anomalies of the soil moisture are summed over the period of the flash drought as indicated in Fig. 4.18. The black dot in each of the panels indicate the location of the landfall of the hurricane.

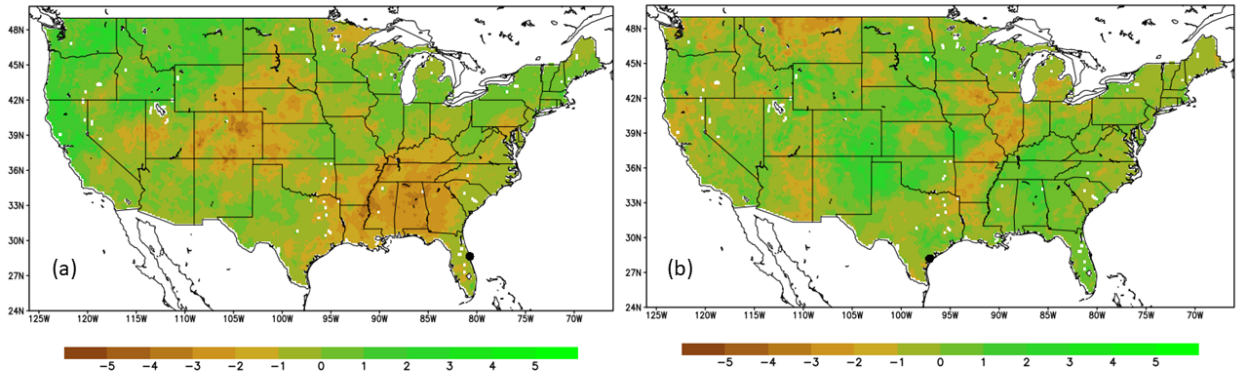

Figure 4.23: The map of the normalized, daily cumulative anomalies of the soil moisture for the flash drought events associated with the landfall of Hurricanes a) Matthew of 2016 and b) Harvey of 2017. The daily normalized anomalies of the soil moisture are summed over the period of the flash drought as indicated in Fig. 4.19. The black dot in each of the panels indicate the location of the landfall of the hurricane.

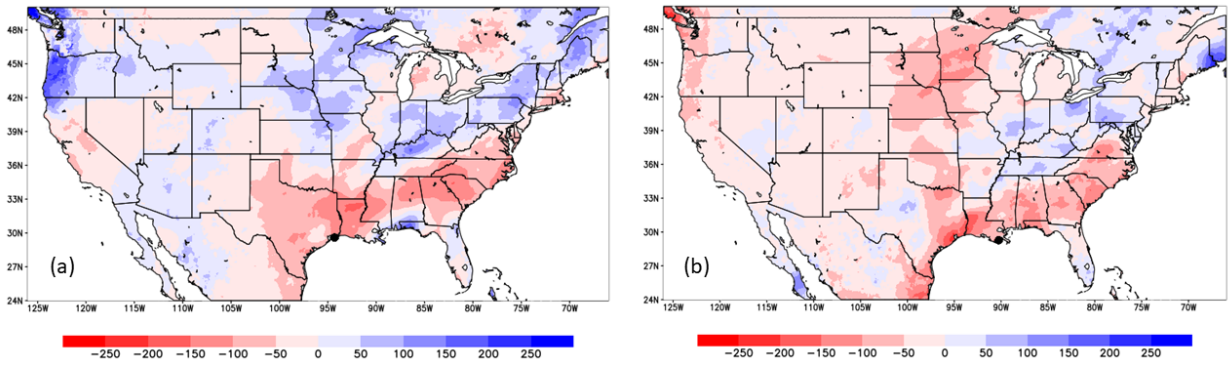

Figure 4.24: The map of the normalized, daily cumulative anomalies of the precipitation for the flash drought events associated with the landfall of Hurricanes a) Humberto of 2007 and b) Isaac of 2012. The daily normalized anomalies of the surface temperature are summed over the period of the flash drought as indicated in Fig. 4.18. The black dot in each of the panels indicate the location of the landfall of the hurricane.

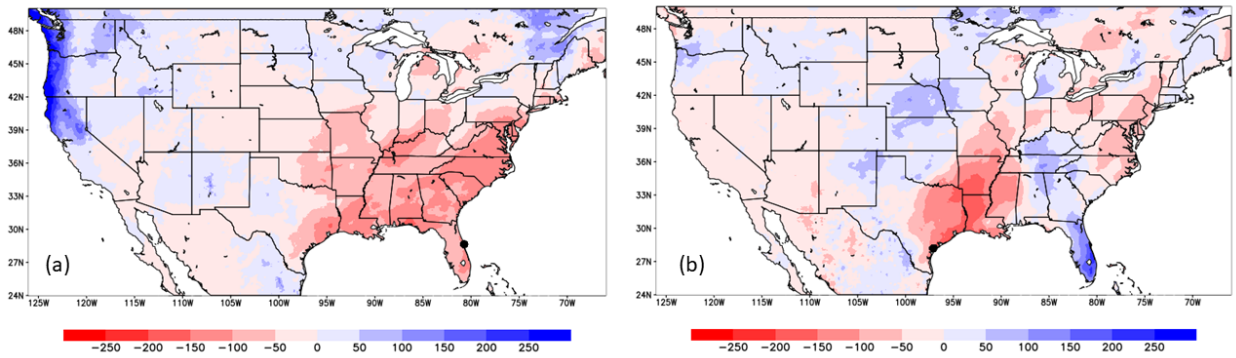

Figure 4.25: The map of the normalized, daily cumulative anomalies of the precipitation for the flash drought events associated with the landfall of Hurricanes a) Matthew of 2016 and b) Harvey of 2017. The daily normalized anomalies of the surface temperature are summed over the period of the flash drought as indicated in Fig. 4.19. The black dot in each of the panels indicate the location of the landfall of the hurricane.

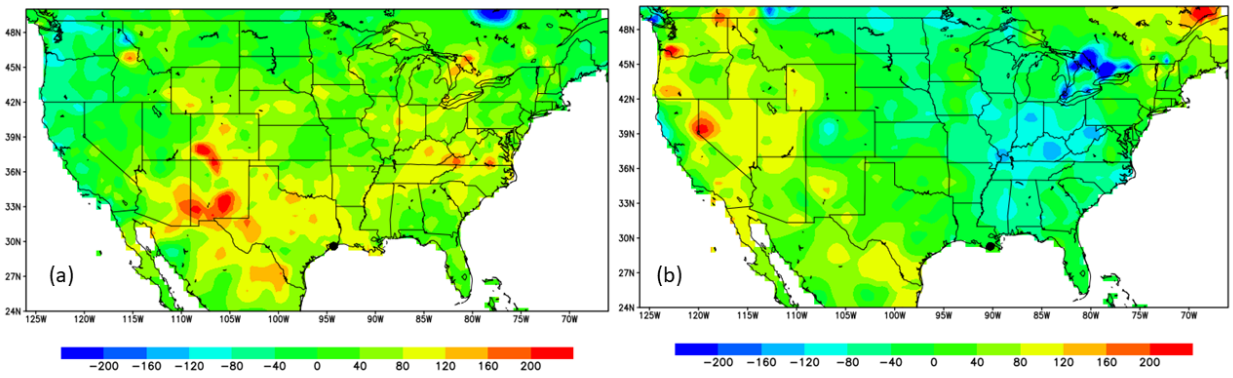

Figure 4.26: The map of the normalized, daily cumulative anomalies of the surface temperature for the flash drought events associated with the landfall of Hurricanes a) Humberto of 2007 and b) Isaac of 2012. The daily normalized anomalies of the precipitation are summed over the period of the flash drought as indicated in Fig. 4.18. The black dot in each of the panels indicate the location of the landfall of the hurricane.

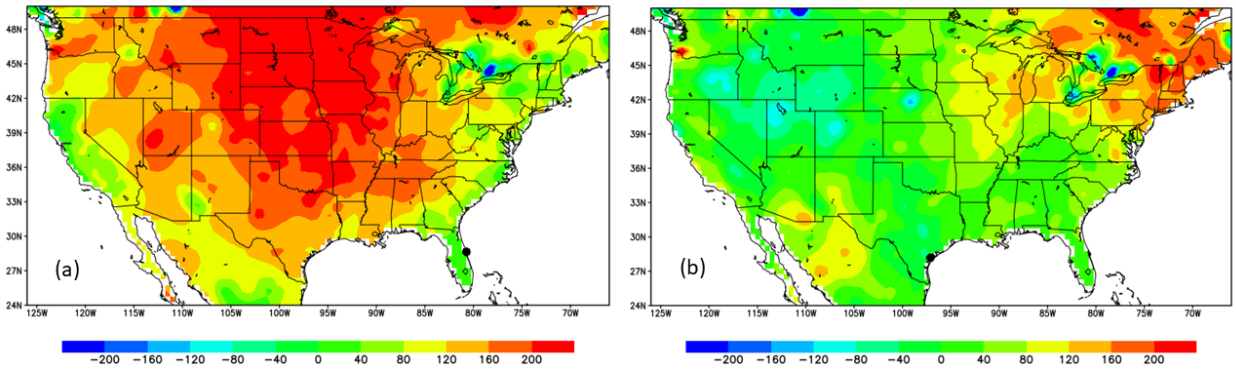

Figure 4.27: The map of the normalized, daily cumulative anomalies of the surface temperature for the flash drought events associated with the landfall of Hurricanes a) Matthew of 2016 and b) Harvey of 2017. The daily normalized anomalies of the precipitation are summed over the period of the flash drought as indicated in Fig. 4.19. The black dot in each of the panels indicate the location of the landfall of the hurricane.

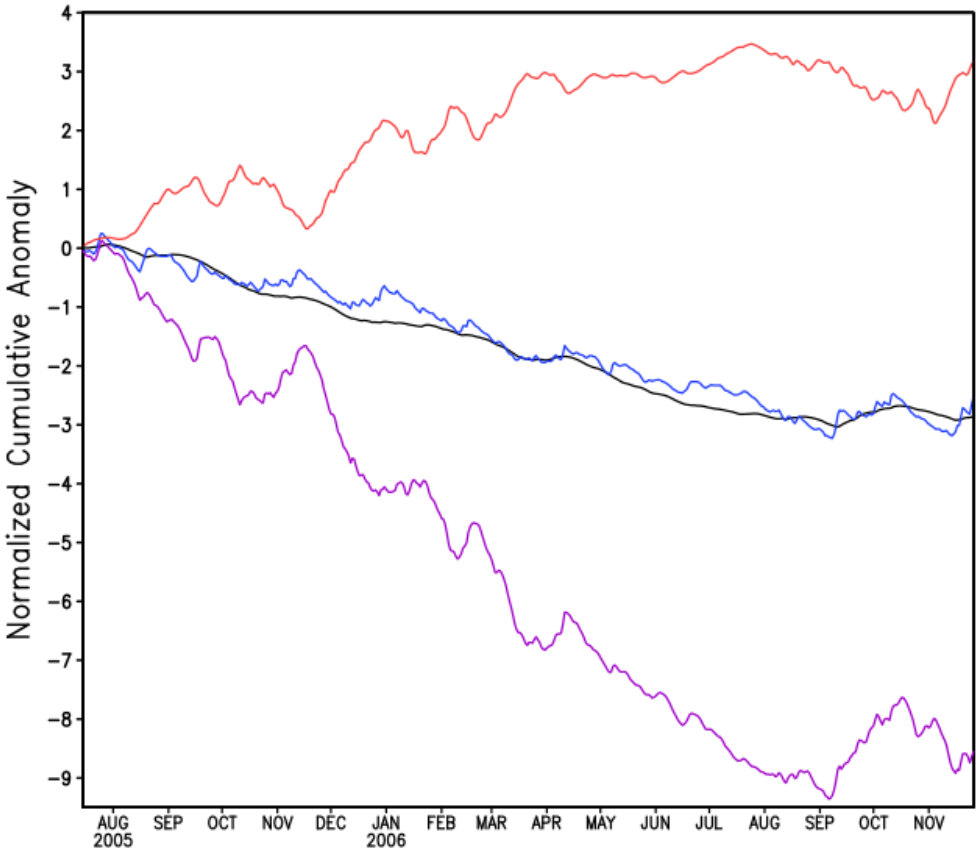

Figure 4.28: Normalized daily cumulative anomaly curves of temperature (red line), soil moisture (black line), precipitation (blue line), and the drought index (purple line) computed over an area of 500 km radius centered on an area near Buras, Louisiana.

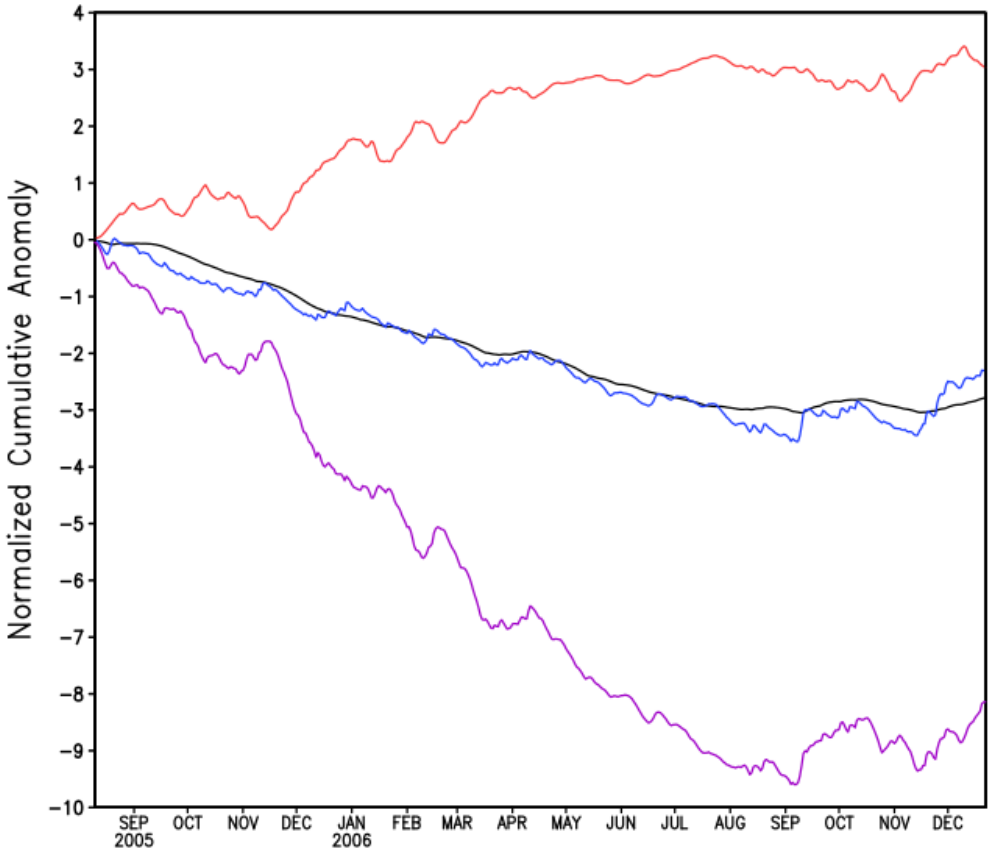

Figure 4.29: Normalized daily cumulative anomaly curves of temperature (red line), soil moisture (black line), precipitation (blue line), and the drought index (purple line) computed over an area of 500 km radius centered on an area near Johnson's Bayou, Louisiana.

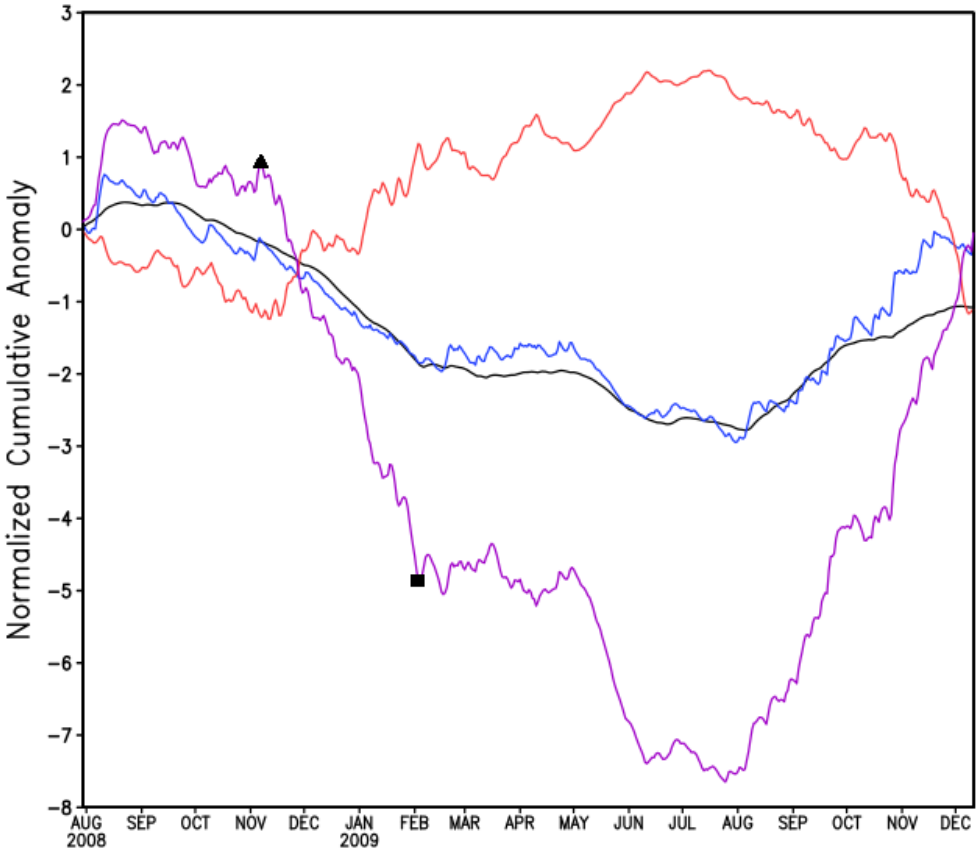

Figure 4.30: Normalized daily cumulative anomaly curves of temperature (red line), soil moisture (black line), precipitation (blue line), and the drought index (purple line) computed over an area of 500 km radius centered around Galveston Island, Texas. The triangle and square indicate the possible start and end of a flash drought event.

REFERENCES

Anderson, M. C. et al., 2013: An intercomparison of drought indicators based on thermal remote sensing and NLDAS-2 simulations with U.S. drought monitor classifications. *J. Hydrometeorol.,* **14**, 1035-1056.

Berg, R., 2013: Tropical Cyclone Report: Hurricane Isaac. 78 pp. Available from: https://www.nhc.noaa.gov/data/tcr/AL092012_Isaac.pdf.

Berg, R., 2008: Tropical Cyclone Report: Hurricane Ike. 55 pp. Available from: https://www.nhc.noaa.gov/data/tcr/AL092008_Ike.pdf.

Berman, M., K. Zezima, and A.C. Davis, 2017: Eight dead after South Florida nursing home's air conditioning fails following Hurricane Irma. Washington Post. Available from: https://www.washingtonpost.com/news/post-nation/wp/2017/09/13/irma-death-toll-rises-as-5-dead-at-south-florida-nursing-home/

Blake, S., D. A. Zelinsky, 2018: Tropical Cyclone Report: Hurricane Harvey. 77 pp. Available from: https://www.nhc.noaa.gov/data/tcr/AL092017_Harvey.pdf.

Brennan, M. J., R. D. Knabb, M. Mainelli, and T. B. Kimberlain, 2007: Annual summary: Atlantic hurricane season of 2007. Mon Wea. Rev., 137, 4061-4088

Chavas, D. R., and K. A. Emmanuel, 2010: A QuikSCAT climatology of tropical cyclone size. *Geophys. Res. Lett.*, **37**, L18816, doi:10.1029/2010GL044558.

Christian, J. I., J. B. Basara, E. D. Hunt, J. A. Otkin, C. Furtado, V. Mishra, X. Xiao, and R. M. Randall, 2021: Global distribution, trends, and drivers of flash drought occurrence. Nat Commun, 12, 6330 (2021). https://doi.org/10.1038/s41467-021-26692-z.

Christian, J. I., J. B. Basara, J. A. Otkin, E. D. Hunt, R. A. Wakefield, P. X. Flanagan, and X. Xiao, 2019: A methodology for flash drought identification: application of flash drought frequency across the United States. J. Hydromet., 20, 833-846, https://doi.org/10.1175/JHM-D-18_0198.1

Dare, R. A., N. E. Davidson, and J. L. McBride, 2012: Tropical cyclone contribution to rainfall over Australia. *Mon. Wea. Rev.*, **140**, 3606-3619, doi:10.1175/MWR-D-11-00340.1.

Dee, D., Uppala, S., Simmons, A., Berrisford, P., Poli, P., Kobayashi, S., et al. (2011). The ERA-Interim reanalysis: Configuration and performance of the data assimilation system. Quarterly Journal of the Royal Meteorological Society, 137(656), 553–597. https://doi.org/10.1002/qj.828

Ford, T. W., and C. F. Labosier, 2017: Meteorological conditions associated with the onset of flash drought in the eastern United States. *Agric. For. Meteor.,* **247**, 414-423, https://doi/org/10.1016/j.agrformet.2017.08.031.

Gelaro, R., W. McCarty, M. J. Suarez, R. Todling, A. Molod, L. Takacs, et al., 2017: The Modern-Era Retrospective Analysis for Research and Applications, Version 2 (MERRA-2). J. Clim., 30(14), 5419-5454.

Hersbach, H., W. Bell, P. Berrisford, A. Horanyi, J. M. Sabater, J. Nicolas, et al. 2019: A reanalysis of the 1944-53 Atlantic hurricane seasons-The first decade of aircraft reconnaissance. J. Clim., 25(13), 4441-4460.

Hoell, A., B. -A. Parker, M. Downey, and coauthors, 2020: Lessons learned from the 2017 flash drought across the U.S. Northern Great Plains and Canadian Prairies. *Bull. Amer. Soc*., https://doi.org/10.1175/BAMS-D-19_0272.1.

Huffman, G.J., Adler, R.F., Bolvin, D.T., Hsu, K., Kidd, C., Nelkin, E.J., Tan, J. and Xie, P., 2019: Algorithm Theoretical Basis Document (ATBD) for global precipitation climatology project version 3.0 precipitation data. MEaSUREs project, Greenbelt, MD.

Hunt, E., M. Svoboda, B. Wardlow, K. Hubbard, M. J. Haynes, and T. Arkebauer, 2014: Monitoring the effects of the rapid onset of drought on non-irrigated maize with agronomic data and climate-based drought indices. *Agric. For. Meteor.*, **191**, 1-11, https://doi.org/10.1016/j.agrformet.2014.02.001.

Jencso, K. et al. 2019. Flash Drought: Lessons Learned from the 2017 Drought Across the U.S. Northern Plains and Canadian Prairies. *NOAA National Integrated Drought Information System*.

Jiang, H., and E. J. Zipser, 2010: Contribution of tropical cyclones to the global precipitation from eight seasons of TRMM data: Regional, seasonal, and interannual variations. *J. Climate*, **23**, 1526-1542, https://doi.org/10.1175/2009JCLI3303.1

Keyantash, John & National Center for Atmospheric Research Staff (Eds.). Last modified 07 Aug 2018. **"The Climate Data Guide: Standardized Precipitation Index (SPI)."** Retrieved from https://climatedataguide.ucar.edu/climate-data/standardized-precipitation-index-spi.

Khouakhi, A., G. Villarini, and G. A. Vecchi, 2017: Contribution of tropical cyclones to rainfall at the global scale. *J. Climate*, **30**, 359-372, https://doi.org/10.1175/JCLI-D-16-0298.1.

Knabb, R. D., D. P. Brown, and J. R. Rhome, 2005: Tropical Cyclone Report: Hurricane Rita. 33 pp. Available from: https://www.nhc.noaa.gov/data/tcr/AL182005_Rita.pdf.

Knabb, R. D., J. R. Rhome, and D. P. Brown, 2005: Tropical Cyclone Report: Hurricane Katrina. 43 pp. Available from: https://www.nhc.noaa.gov/data/tcr/AL122005_Katrina.pdf.

Lee, M.-H., C.-H. Ho, and J.-H. Kim, 2010: Influence of tropical cyclone landfalls on spatiotemporal variations in typhoon season rainfall over South China. *Adv. Atmos. Sci.,* **27**, 443-454, https://doi.org/10.1007/s00376-009-9106-3.

Liu, Z., 2016: Comparison of integrated multisatellite retrievals for GPM (IMERG) and TRMM multi-satellite precipitation analysis (TMPA) monthly precipitation products: Initial results. J. Hydrometeorol., 17, 777–790

McEvoy, D. J. et al., 2016: The evaporative demand drought index. Part II: CONUS-wide assessment against common drought indicators. *J. Hydrometeorol.*, **17**, 1763-1779.

Mei, R. and Wang, G. Summer land-atmosphere coupling strength in the United States: comparison among observations, reanalysis data, and numerical models. *J. Hydrometeorol.* **13**, 1010-1022 (2012).

Misra, V., C. B. Jayasankar, P. Beasley, A. Bhardwaj, 2022: Operational Monitoring of the Evolution of Rainy Season over Florida. *Frontiers in Climate*.

Misra, V., 2020: Regionalizing Global Climate Variations: A Study of the Southeastern US Regional Climate. Elsevier, 324 pp, ISBN:978-0-12-821826-6.

Mo, K. C., and D. P. Lettenmaier, 2015: Heat wave flash droughts in decline. *Geophys. Res. Lett.,* **42**, 2823-2829, https://doi.org/10.1002/2015GL064018.

NASA, 2021: README Document for SMERGE Root-zone Soil Moisture Data Product Version 2.0. Accessed 23 January 2022, https://hydro1.gesdisc.eosdis.nasa.gov/data/SMERGE/SMERGE_RZSM0_40CM.2.0/doc/README_SMERGE2.pdf

NASA, 2021: IMERG Final Run. Accessed 8 July 2021, https://gpm.nasa.gov/taxonomy/term/1417

Nguyen, H. et al., 2019: Using the evaporative stress index to monitor flash drought in Australia. *Environ. Res. Lett.*, **14**, 064016.

NOAA, 2020: Climate Prediction Center Global Daily Temperature. NOAA, accessed 19 January 2022, psl.noaa.gov/data/gridded/data.cpc.globaltemp.html

NOAA, n.d.: DROUGHT: Monitoring Economic, Environmental, and Societal Impacts. Accessed 23 January 2022, https://www.ncdc.noaa.gov/news/drought-monitoring-economic-environmental-and-social-impacts

Otkin, J., M. Svoboda, E. Hunt, T. Ford, M. Anderson, C. Hain, and J. Basara, 2018: Flash Droughts: A Review and Assessment of the Challenges Imposed by Rapid-Onset Droughts in the United States. *Bull.Amer.Meteor.Soc.,* **99**, 911-919, https://doi.org/10.1175/BAMS-D-17-0149.1

Otkin, J. A., M. C. Anderson, C. Hain, I. Mladenova, J. Basara, and M. Svoboda, 2013: Examining flash drought development using the thermal infared based evaporative stress index. *J. Hydrometeor.,* **14**, 1057-1074, https://doi.org/10.1175/JHM-D-12-0144.1

Prat, O. P., and B. R. Nelson, 2013: Mapping the world's tropical cyclone rainfall contribution over land using the TRMM Multi-satellite Precipitation Analysis. *Water Resour. Res.*, **49**, 7236-7254, doi:10.1002/wrcr.20527.

Retchless, D.; Frey, N.; Wang, C.M.; Hung, L.S.; Yarnal, B. Climate extremes in the united states: Recent research by physical geographers. *Phys. Geogr.* **2014**, *35*, 3-21.

Rui, H. and J. Dong, 2021: README Document for SMERGE Root-zone Soil Moisture Data Product Version 2.0. Available from: https://hydro1.gesdisc.eosdis.nasa.gov/data/SMERGE/SMERGE_RZSM0_40CM.2.0/doc/README_SMERGE2.pdf

Rui, H. and D. Mocko, 2021: README Document for North American Land Data Assimilation System Phase 2 (NLDAS-2) Products. Available from: https://hydro1.gesdisc.eosdis.nasa.gov/data/NLDAS/README.NLDAS2.pdf

Schenkel, B. A. and R. E. Hart, 2015: An Examination of the Thermodynamic Impacts of Western North Pacific Tropical Cyclones on Their Tropical Tropospheric Environment. *J. Climate*., **28**, 7529-7560, https://doi.org/10.1175/JCLI-D-14-00780.1.

Scoccimarro, E., S. Gualdi, A. Bellucci, D. Peano, A. Cherchi, G. A. Vecchi, and A. Navarra, 2020: The typhoon-induced drying of the Maritime Continent. PNAS. https://doi.org/10.1073/pnas.1915364117.

Seneviratne, S. I., T. Corti, E. L. Davin, M. Hirschi, E. B. Jaeger, I. Lehner, B. Orlowsky, and A. J. Teuling, 2010: Investigating soil moisture-climate interactions in a changing climate: A review. *Earth-Sci. Rev.,* **99**, 125-161, https://doi.org/10.1016/j.earscirev.2010.02.004.

Shi, W., 2021.: Global Daily Surface Air Temperature Analyses. 8 pp. Available from: https://psl.noaa.gov/data/gridded/data.cpc.globaltemp.html

Sobel, A. and S. J. Camargo, 2005: Influence of Western North Pacific Tropical Cyclones on their large-scale environment. J. Atmos. Sci., 62 (9), 3396-3407

Stewart, S. R., 2017: Tropical Cyclone Report: Hurricane Matthew, 96 pp. Available from https://www.nhc.noaa.gov/data/tcr/AL142016_Matthew.pdf.

Tan, J., G.J. Huffman, D.T. Belvin, E.J. Nelkin, 2019: IMERG V06: Changes to the Morphing Algorithm. *J. Atmos. Ocean. Technol.,* **36**(12), 2471-2482. *doi:10.1175/JTECH-D-19-0114.1*

Tang, G.; Ma, Y.; Long, D.; Zhong, L., Hong, Y., 2016: Evaluation of GPM Day-1 IMERG and TMPA Version-7 legacy products over Mainland China at multiple spatiotemporal scales. J. Hydrol., 533, 152-167.

Villarini, G., D. A. Lavers, E. Scoccimarro, M. Zhao, M. F. Wehner, G. A. Vecchi, T. R. Knutson, and K. A. Reed, 2014b: Sensitivity of tropical cyclone rainfall to idealized global-scale forcings. *J. Climate*, **27**, 4622-4641, doi:10.1175/JCLI-D-13-00780.1.

Villarini, G.; Smith, J.A.; Baeck, M.L.; Krajewski, W.F. Examining flood frequency distributions in the Midwest US. *J. Am. Water Resour. Assoc.* **2011**, *47*, 447-463.

Wang, L., X. Yuan, Z. Xie, P. Wu, and Y. Li, 2016: Increasing flash droughts over China during the recent global warning hiatus. *Sci. Rep.*, **6**, 30571, https://doi.org/10.1038/srep30571.

Xu, F.; Guo, B.; Ye, B.; Ye, Q.; Chen, H.; Ju, X.; Guo, J., 2019: Wang, Z. Systematical evaluation of GPM IMERG and TRMM 3B42V7 precipitation products in the Huang-Huai-Hai Plain, China. Remote Sens., 11, 697.

Yuan, X., L. Wang, and E. F. Wood, 2018: Anthropogenic intensification of Southern African flash droughts as exemplified by the 2015/16 season. *Bull. Amer. Meteor. Soc.,* **99**, S86-S90, https://doi.org/10.1175/BAMS-D-17-0077.1.

Zhou, Y., Matyas, H. Li, and J. Tang, 2018: “Conditions associated with rain field size for tropical cyclones landfalling over Eastern United States”. Atmos. Res., 214, doi:10.1016/j.atmosres.2018.08.019

BIOGRAPHICAL SKETCH

Tyler Sherrod was born in St. Mary's, Georgia in 1998. He moved to Melbourne, FL in the summer of 2004 and began developing a passion for meteorology upon witnessing the 2004 hurricane season. Upon graduating from Viera High School in 2016, Tyler enrolled at the University of Central Florida to study aerospace engineering. Quickly realizing that his true passion was in meteorology, he transferred to Florida State University in 2018 after earning his Associate of Arts degree at the University of Central Florida. Tyler graduated with his Bachelor of Science in Meteorology in 2020 and enrolled in graduate school at Florida State University the following semester, working with Dr. Vasu Misra for his thesis work. With the submission of this thesis, Tyler will be set to graduate in the Spring of 2022. After graduation, he plans to enter the meteorological work force.